BMC Medicine

RESEARCH

Open Access

Enhancing anti-CD3 mAb-mediated diabetes remission in autoimmune diabetes through regulation of dynamin-related protein 1(Drp1)-mediated mitochondrial dynamics in exhausted CD8$^+$T-cell subpopulations

Ruiling Zhao[1†], Zhangyao Su[1†], Junjie Gu[2], Hang Zhao[1], Lingling Bian[1,3], Yin Jiang[1], Yun Cai[1], Tao Yang[1], Yong Gu[1*] and Xinyu Xu[1*]

Abstract

Background Antigen-specific immunotherapy shows potential for inducing long-term immune tolerance in type 1 diabetes (T1D), yet its clinical application is hampered by uncertainty regarding dominant epitopes. Conversely, non-antigen-specific treatments such as anti-CD3 monoclonal antibodies (mAbs) present a more straightforward approach but struggle to maintain tolerance after treatment. Addressing these issues is critical for advancing T1D therapies.

Methods The phenotypic and metabolic properties of two subsets of exhausted CD8$^+$ T cells were analyzed in both humans and NOD mice. T-cell receptor (TCR) diversity and Bulk RNA sequencing provided insights into the transcriptomic profiles and TCR reactivity of these cells. Mechanistic studies were conducted using the HEK-293 T cell line and primary cells. Single-cell RNA sequencing (scRNA-seq) was applied to evaluate the characteristics of different CD8$^+$ T cell subsets following two types of immunotherapies. In NY8.3 mice, the effect of mitochondrial fission inhibitors on immunotherapy results was evaluated. Final validation was carried out with peripheral blood mononuclear cells (PBMCs) from T1D patients.

Results Our study reveals the diversity of two distinct exhausted CD8$^+$ T cell subsets in T1D through flow cytometry, highlighting unique clinical features, phenotypes, and functions. Notable differences in TCR reactivity and metabolic pathways between these subsets were identified through TCR sequencing and transcriptomic analyses in NOD mice. Both antigen-specific and non-antigen-specific stimuli produced unique exhausted CD8$^+$ T cell subsets. Our research identified leucine-rich repeat kinase 2 (Lrrk2) as a key regulator of mitochondrial fission, influencing the interconversion of exhausted CD8$^+$ T cell subsets by phosphorylating dynamin-related protein 1 (DRP1) at serine 637 (Ser637) and serine 616 (Ser616). scRNA-seq confirmed that antigen-specific immunotherapy effectively suppresses T cell

†Ruiling Zhao and Zhangyao Su contributed equally to this work.

*Correspondence:
Yong Gu
yong.gu@njmu.edu.cn
Xinyu Xu
drxinyuxu@njmu.edu.cn
Full list of author information is available at the end of the article

signaling, induces exhaustion, and promotes the development of terminally exhausted T (TEX) cells. Mitochondrial division inhibitor 1 (Mdivi-1) enhanced the therapeutic effect of anti-CD3 mAb treatment by promoting the development of more TEX cells.

Conclusions Our results point to a new immunotherapeutic approach that targets exhausted $CD8^+$ T cells' energy metabolism, offering valuable insights for advancing clinical strategies in T1D therapy.

Keywords Exhausted T cell, Immune tolerance, Immunotherapy, CD3 mAb, Autoimmunity

Background

Type 1 diabetes is an autoimmune condition that specifically targets and destroys pancreatic β-cells [1–3], transforming from a life-threatening condition to a manageable chronic disease primarily treated with exogenous insulin [4]. Nevertheless, there remains a critical need for innovative therapies aimed at halting or delaying the loss of functional β cell mass [5, 6]. Antigen-specific immunotherapy strives to induce peripheral immune tolerance without the extensive immune suppression associated with current monoclonal antibody treatments. However, the variability in islet autoantigens among individuals and disease stages presents a significant obstacle to achieving effective immune tolerance induction. While promising results have been observed in NOD mouse models concerning antigen-induced immune tolerance, translating these outcomes into effective standalone therapies for humans has proven challenging [7, 8]. Several immunosuppressive drugs have demonstrated partial efficacy, particularly in newly diagnosed individuals, by preserving β-cell function [9–12]. In particular, otelixizumab and teplizumab, two anti-CD3 mAbs, have demonstrated encouraging outcomes in patients with T1D [13, 14]. Recently, the Food and Drug Administration (FDA) approved teplizumab, marking it as the first-in-class drug designed to prevent T1D [15]. However, despite these advancements, none of these approaches have achieved durable immune tolerance or sustained insulin independence over the long term [11, 16–18].

$CD8^+$ T-cell exhaustion is a type of T-cell failure that occurs in both cancer and persistent infections [19–21]. These cells gradually lose their ability to secrete IL-2, destroy target cells, and release proinflammatory cytokines like TNF-α and IFN-γ as they break down [22]. Changes in metabolic fitness altered expression and usage of important transcription factors, and persistent overexpression of inhibitory receptors are all associated with this dysfunction [23–25]. Notably, exhausted $CD8^+$ T-cell populations display considerable heterogeneity [26, 27]. Two primary groups of exhausted $CD8^+$ T-cell subsets have been distinguished: terminally exhausted T (TEX) cells, which maintain superior cytotoxicity but have a lower long-term survival rate, and progenitor exhausted T (TPEX) cells, which are more polyfunctional and can survive in the absence of antigen [27]. In patients with autoimmune disorders, transcriptomic profiling has discovered a hallmark of $CD8^+$ T-cell exhaustion that correlates with a less severe disease phenotype [28]. Recent research has identified exhausted $CD8^+$ T cells within the pancreatic islets, displaying markers as TIM-3, TOX, PD-1, and TIGIT in human and NOD mice [29, 30]. Increased response to immunosuppressive therapies or better prognostic outcomes has been related with elevated levels of exhausted $CD8^+$ T-cell in T1D [31–33]. Nevertheless, it is still unknown precisely how certain exhausted $CD8^+$ T-cell subsets contribute to T1D pathogenesis. Furthermore, little is known about the developmental biology and underlying processes that control the generation, persistence, and responsiveness of $CD8^+$ exhausted T-cell subsets to various immunotherapies in T1D.

The relationship between various parts of T-cell response and bioenergetic metabolism has gained more attention in recent years [34]. This understanding has prompted new considerations regarding the potential for modulating T-cell responses [35]. Our analysis aimed to discern whether TPEX and TEX cells manifest different cellular states and metabolic characteristics within the context of T1D. Additionally, we explored the presence of distinct phenotypes among exhausted $CD8^+$ T-cell subsets following different immunotherapy approaches. Lastly, we evaluated the potential of combining immunotherapy with metabolic interventions as a novel strategy to effectively harness exhausted T cells and improve clinical outcomes in T1D immunotherapy.

Methods

Patients/participants and data collection

One hundred eleven autoantibody-negative healthy individuals and 87 patients with T1D were recruited from the First Affiliated Hospital of Nanjing Medical University in Jiangsu, China. The overall 28-month period for blood sample collection is from August 2019 to December 2021. The American Diabetes Association's criteria were used to diagnose T1D patients [36]. Patients and controls suffering from other autoimmune disorders and those with irrelevant chronic diseases were not included. The radio-immunoprecipitation assay (RIPA) was used

to identify islet autoantibodies (zinc transporter 8 antibody (ZnT8A), glutamic acid decarboxylase 65 antibody (GAD65A), and protein tyrosine phosphatase 2 antibody (IA2A)). All patients tested positive for autoantibodies to at least one antigen. All patients were treated with insulin, and no other diabetes-related or immunotherapy medications were administered. Participants in the study provided written informed consent prior to their inclusion. The Human Ethics Committee at the First Affiliated Hospital of Nanjing Medical University provided ethical approval for the study, including the consent process.

Biochemical and clinical tests

Venous blood specimens were collected after an overnight fast to assess various metabolic parameters. The ARIANT II Hemoglobin Test System (Bio-Rad) was used to measure hemoglobin A1c (HbA1c). Plasma glucose and biochemical levels were analyzed using a Beckman AU5800 automated analyzer (Beckman Coulter).

Mice

Female NOD/ShiLtJ, TcraTcrbNY8.3 (8.3-NOD or NY8.3), and NOD/SCID mice weighing 20–25 g were purchased from the Jackson Laboratory and kept in specific pathogen-free environments (12-h light/dark cycle; 20–26 °C; 40–60% humidity) at the GemPharmatech Co., Ltd. (Nanjing, China). Mice were acclimated for 1 week and simultaneously randomized to different groups following simple randomization. The Institutional Animal Care and Use Committee's (IACUC) guidelines were followed when conducting the experiments at Nanjing Medical University.

Flow cytometry

PBMCs were isolated from heparinized tubes following the manufacturer's guidelines using a Lymphoprep™ (Nycomed) gradient. The spleen and draining lymph nodes of mice were used to separate lymphocytes. After performing surface immunostaining on approximately 10^6 cells at a time, the cells were treated for 20 min at 4 °C with a panel of fluorochrome-labeled antibodies (the antibodies used are listed in the key resources table). Fifty nanograms per milliliter phorbol myristic acid (PMA, MedChemExpress), 1 μg/mL ionomycin (MedChemExpress), and 10 μg/mL Brefeldin A (MedChemExpress) were used to stimulate cells for 5 h before they were stained with antibodies to the surface receptors to evaluate intracellular cytokine production. Fixation and Permeabilization Kit (Nordic-Mubio) was used for fixation and permeabilization, followed by intracellular cytokine labeling. Following instructions provided by the manufacturer, intracellular transcription factor labeling was performed with the FOXP3/Transcription Factor Staining Buffer Set (eBioscience). All samples were collected with a FACS Aria II Sorp flow cytometer (BD Biosciences), and the data was evaluated using FlowJo software.

Evaluation of human T cell function in vitro

CFSE-labeled fresh PBMCs were plated in a round-bottomed 96-well plate with 10 μg/ml plate-bound anti-CD3 antibody (BioLegend) and 2 μg/ml soluble anti-CD28 antibody (BioLegend) for 3 days in RPMI 1640 complete medium to test for proliferation function. Cells were then collected and stained. PBMCs were first treated with 10 μg/ml plate-bound anti-CD3 antibody and 2 μg/ml soluble anti-CD28 antibody overnight, then stained with the Zombie VioletTM Fixable Viability Kit (BioLegend) as directed by the manufacturer for apoptosis level, followed by washing and surface staining. Finally, cells were treated with Annexin V-FITC (4A Biotech) for 5 min at room temperature, shielded from light, and analyzed within 1 h after binding buffer was added.

Bulk RNA-seq and bioinformatics analysis

TPEX, TEX, and T effector (TEFF) cells were purified for total RNA extraction using the RNeasy Mini Kit (Qiagen, Germany). Paired-end libraries were generated using the TruSeq® RNA Sample Preparation Kit (Illumina, USA), following the guidelines provided in the TruSeq® RNA Sample Preparation Guide. In short, Poly-T oligo-conjugated magnetic beads were employed to selectively isolate mRNA molecules with poly-A tails. To verify the insert size and determine the mole concentration, purified libraries were measured using the Qubit® 2.0Fluorometer (Life Technologies, USA) and confirmed using the Agilent 2100 bioanalyzer (Agilent Technologies, USA). After the library was diluted to 10 pM, the cluster was produced using cBot and sequenced on the Illumina HiSeq X-ten (Illumina, USA). The library's creation and sequencing were completed at Shanghai Biotechnology Corporation.

Sequencing data processing are provided in Additional file 1: Supplementary Materials and Methods [37–43] for details.

Conversion between TPEX, TEX, and TEFF cells

TPEX, TEX, and TEFF cells from NOD mice aged 8–13 weeks were sorted by a BD Biosciences FACSAria II. CD3-depleted splenocytes were isolated from NOD mice using flow cytometric sorting, and then treated with 25 μg/ml Mitomycin C (MedChemExpress) for 30 min at 37 °C [44, 45]. Following incubation, the cells were thoroughly washed with PBS before being used as feeder cells. Methods were performed as previously described [46]. For induction of TPEX conversion into TEFF and

TEX conversion into TPEX, we plated sorted TPEX or TEX cells at 1×10^6 cells/ml and 96-well round-bottom plate with an equal number of APCs that had already been treated with Mitomycin C in RPMI 1640 complete medium with 100 ng/ml soluble anti-CD3 antibody and 200 ng/ml soluble anti-CD28 antibody, with or without 6000 IU/ml IL-2. The medium was changed after 5 days. After 1 week of incubation, cells were treated with 10 μg/mL Brefeldin A for the last 5 h before collection to prepare them for assays of cell surface markers and intracellular cytokines. For induction of TPEX differentiation to TEX, overall steps were the same as above. However, instead of the standard culture conditions, RPMI 1640 complete medium was utilized supplemented with 100 ng/ml anti-CD3 antibody, 200 ng/ml anti-CD28 antibody, and optionally 100 IU/ml IL-2 and 400 IU/ml IL-10.

TCR repertoires

NOD mice aged 8–13 weeks ($n=3$/group) were sacrificed and lymphocytes were isolated. After staining, TPEX and TEX were labeled in vitro. Using a FACSAria II, cells were sorted immediately into buffer RLT (Qiagen) with 1% 2-mercapto-ethanol (Sigma) added. Sorted samples were kept at − 80 °C for analysis using iRepertoire (Huntsville, AL), which identified Vβ-chain utilization of in vivo-labeled exhausted $CD8^+$ T cell subsets. IR methodology is explained by Niu et al. [47].

T cell sorting

Lymphocytes were first separated from the lymph nodes and spleens of NOD mice aged 8–13 weeks. Before isolating $CD8^+$ T lymphocytes, the Mouse $CD8^+$ T Lymphocyte Enrichment Set (BD Biosciences, USA) was used for cell purification following the manufacturer's protocol. The cell types detected using fluorescently labeled anti-CD8, anti-PD-1, anti-CD44, anti-Slamf6, anti-TIM-3, and anti-$CD8^+$Slamf6$^+$TIM-3$^-$ (TPEX), $CD8^+$Slamf6$^-$TIM-3$^+$ (TEX), and $CD8^+$CD44$^+$PD-1$^-$ (TEFF) cells were subsequently sorted by a FACS Aria II Sorp flow cytometer (BD Biosciences).

Antigen stimulation of mouse lymphocytes in vitro

$CD8^+$ T cells were isolated from NY8.3 mice aged 6–8 weeks and plated at a density of 1×10^6 cells/mL in a 96-well round-bottom plate. Each well contained an equal number of antigen-presenting cells and was cultured in RPMI 1640 complete medium. To stimulate the T cells, the cultures were either treated with 10 μmol/L of $IGRP_{206–214}$ peptide or exposed to 5 μg/mL of plate-bound anti-CD3 antibody (BioLegend) and 2 μg/mL of soluble anti-CD28 antibody (BioLegend). Cells were cultured at 37 °C for 72 h before being collected for subsequent examination.

Detection of mitochondrial ETC protein and superoxide levels

Targeted cells were first surface-stained and subsequently fixed using the FOXP3/Transcription Factor Staining Buffer Set (eBioscience) to facilitate the detection of mitochondrial electron transport chain (ETC) proteins. The cells were then incubated for 15 min at room temperature, in the dark, with anti-ATP5O (Abcam) and anti-Cytochrome C (BioLegend) antibodies. After surface labeling, the targeted cells were incubated at 37 °C for 15 min, in the dark, with 5 μM MitoSOX™ Red (Thermo Fisher) to assess mitochondrial superoxide levels.

Determination of metabolic characteristics

Prior to surface staining, lymphocytes were resuspended and incubated at 37 °C for 20 min, protected from light, with the following dyes: 20 μM 2-NBDG (Thermo Fisher), 1 μM BODIPY™ 500/510 C1, C12 (Thermo Fisher), or 100 nM MitoScene™ 633 (MTR, US EVERBRIGHT) in pre-warmed RPMI 1640 complete medium, or 100 nM MitoTracker™ Green FM (MTG, Thermo Fisher) in pre-warmed RPMI 1640 medium. Cells were then stained with 1 μg/mL BODIPY™ 493/503 (Thermo Fisher) for lipid droplet analysis. After a 1 h incubation at 4 °C in the dark, surface staining was performed. For CD36 analysis, Anti-CD36 (BioLegend) was added with the other antibodies during surface staining.

Electron microscopy

The sorted cells were preserved in cacodylate buffer (0.1 M, pH 7.4) containing 2.5% paraformaldehyde and 25% glutaraldehyde for transmission electron microscopy (TEM). To enhance contrast, the samples were post-fixed for 2 h with 1% osmium tetroxide, followed by staining with 2% uranyl acetate (wt/vol.) in double-distilled water. Samples were embedded in EPON 812 after multiple washings and graded alcohol (50, 70, 90, and 100%) dehydration. They were subsequently processed into ultrathin sections of 60–80 nm using a Leica ultramicrotome EM UC6 (Leica). A JEOL JEM-1400Flash (JEOL) transmission electron microscope operating at an accelerating voltage of 80 kV was used to observe cell structures. Quantification was performed on the number of mitochondria per cell and the length of all the mitochondrial cristae per mitochondrion.

Mitochondrial suppression in vitro

After isolation from NY8.3 mice aged 6–8 weeks, $CD8^+$ T cells were cultivated in an activating media using

$IGRP_{206–214}$ peptide or anti-CD3/anti-CD28 with 10 μM Oligomycin A (MedChemExpress)/ 1 μM Antimycin A (Maokang Biotechnology), 200 μM Mdivi-1 (MedChemExpress), or 10 μM Oligomycin A/1 μM Antimycin A/200 μM Mdivi-1 and incubated for 4 h in vitro for cell staining and detection.

Human PBMCs were obtained from T1D patients and then stimulated with 10 μg/ml plate-bound anti-CD3 and 2 μg/ml soluble anti-CD28 under the culture conditions described above, and assayed after 12 h incubation in vitro.

Cell transfection

293 T cells were cultured in Dulbecco's modified Eagle's medium supplemented with 10% fetal bovine serum (Hyclone, Logan, UT). To generate cell lines expressing the leucine-rich repeat kinase 2 (*Lrrk2*) gene, 293 T cells were initially transfected with the *Lrrk2* plasmid. Subsequently, *Lrrk2* knockdown was achieved by transfecting the cells with an *Lrrk2*-specific plasmid followed by shRNA-mediated interference.

Quantitative real-time PCR(qRT-PCR)

qRT-PCR was used to evaluate mRNA expression levels. To put it briefly, total RNA was extracted using Trizol (Invitrogen, USA), and cDNA synthesis was performed with the PrimeScript RT Reagent Kit (Takara, Japan). Quantitative PCR was then performed using SYBR Green RT-PCR Mix on an Applied Biosystems QuantStudio system (Thermo Fisher Scientific, USA).

Western blot

Proteins were separated using SDS-PAGE, and protein expression under equivalent loadings of each sample was then examined using electrophoretic transfer, immunoblotting, and chemiluminescent detection. The following antibodies and their respective dilutions were used: anti-Lrrk2 (clone MJFF2 (c41-2), Abcam, ab133474) at 1:10,000; anti-Drp1 (clone D6C7, Cell Signaling Technology (CST), 8570S) at 1:1000; anti-phospho-Drp1 (Ser637) (clone D3A4, CST, 6319S) at 1:1,000; anti-phospho-Drp1 (Ser616) (clone D9A1, CST, 4494S) at 1:1000; and anti-β-actin (clone 8H10D10, CST, 3700S) at 1:1000.

Single-cell library preparation and sequencing

FACSAria II cell sorter (BD Biosciences) was used to isolate $CD8^+$ T cells from the spleen and lymph nodes of NY8.3 mice treated with $IGRP_{206–214}$ or anti-CD3 mAb. The Singleron Matrix® Single Cell Processing System loaded 2×10^5 cells/mL with PBS (HyClone) into microwell chips. After the removal of barcoding beads from the microwell chips, the captured mRNA was subjected to reverse transcription and PCR amplification to generate complementary DNA (cDNA). Sequencing adapters were subsequently used to segment and ligate the amplified cDNA. The GEXSCOPE® Single Cell RNA Library Kits (Singleron) procedure was followed in the construction of the scRNA-seq libraries [48]. After dilution to 4 nM, the separate libraries were combined and sequenced on an Illumina NovaSeq 6000, using 150-bp paired-end reads.

Sequencing data processing are provided in Additional file 1: Supplementary Materials and Methods for details.

Immunomodulation of mitochondrial inhibitors with antigens in vitro

Following $CD8^+$ T cell isolation from NY8.3 mice aged 6–8 weeks, the cells were plated at 1×10^6 cells/ml in a 96-well round-bottom plate. On day 0, the cells were initially activated by using 10 μmol/L $IGRP_{206–214}$ peptide in RPMI 1640 complete medium + 25 U/ml IL-2. After 24 h (day 1), the cells were treated with 2 μg/million cells InVivoMAb anti-mouse CD3ε (Bio X Cell) or 10 μmol/L $IGRP_{206–214}$ peptide, with or without 10 μM Oligomycin A/1 μM Antimycin A/200 μM Mdivi-1 in fresh RPMI 1640 complete medium + 25 U/ml IL-2. After 48 h (day 3), cells were divided in half, so that each group now had eight wells instead of four and the exhausted growth medium was exchanged for fresh medium for each group. After another 48 h, Brefeldin A (10 μg/mL) was added 5 h before sample collection and cytokine assays.

Human PBMCs were isolated from T1D patients and then activated with 10 μg/ml plate-bound anti-CD3 and 2 μg/ml soluble anti-CD28. The cells were seeded into a 96-well round-bottom plate at a concentration of 1×10^6 cells/ml on day 0. Fresh medium + 25 U/ml IL-2 containing 2 μg/million cells InVivoMAb anti-human CD3 (Bio X Cell) with or without 10 μM Oligomycin A/ 1 μM Antimycin A/ 200 μM Mdivi-1 was used to replace the old medium after 24 h (day 1). After another 48 h (day 3), each group of cells was divided into two halves and the medium was exchanged for fresh, corresponding medium. On day 5, 10 μg/mL Brefeldin A was added 5 h prior to sample collection and cytokines assays.

Adoptive transfer experiments and in vivo treatment

For adoptive transfer experiments, 6×10^5 $CD3^+CD8^+CD44^+PD\text{-}1^-$ TEFF cells sorted from NY8.3 female mice aged 6 weeks and resuspended in PBS were administered intravenously to NOD/SCID recipients for adoptive transfer assessments. Then recipients randomly received either 10 μg of InVivoMAb anti-mouse CD3ε (Clone: 145-2C11, Bio X Cell) i.v. per day for 5 days [49], or were administered 40 μg of $IGRP_{206–214}$ peptide in 20 μl sterile PBS (20 μg in 10 μl per nostril) intranasally

per day for 3 days [50]. Exhausted $CD8^+$ T cell subpopulations were assayed in NOD/SCID mice at 5 or 15 days after the drug administration.

For in vivo treatment, there were 3 dosing regimens: (1) 10 μg CD3 mAb i.v. per day for 5 days; (2) 40 μg $IGRP_{206–214}$ peptide i.n. daily for 3 days; (3) 10 μg CD3 mAb, 0.125 mg/kg Oligomycin A [51], 5 mg/kg Antimycin A [52], and 1 mg/kg Mdivi-1 [53] i.v. per day for 5 days. Controls were given PBS treatment. NY8.3 female mice aged 6 weeks were treated randomly with the administration regimens above and blood glucose was measured daily to monitor for diabetes. After 60 days, non-diabetic mice were sacrificed and observed for insulitis and cellular phenotype. Diabetic NY8.3 mice were also treated with the above administration and monitored blood glucose daily for 30 days.

Diabetes assessment and histology

Blood glucose levels were tested using a Contour blood glucose meter (Terumo), and diabetes was identified through venous blood analysis. Two readings in a row above 13.9 mM were considered diabetes. The methods used for histological investigation included staining 5-μm sections with hematoxylin and eosin and fixation of the pancreas in 10% (vol./vol.) buffered formalin. Pancreatitis was then detected by blindly scoring ten pancreatic slices. Images were taken with a Zeiss Axio Vert A1 microscope, and image analysis was performed using Adobe Illustrator CS2. The scoring system used was as follows: 0 = no infiltration, 1 = 0 to 25%, 2 = > 25 to 75%, and 3 = > 0.75%.

Statistical analysis

The Mann–Whitney *U* test was used for comparisons of non-normally distributed data, while the unpaired Student's *t* test was applied to data with a normal distribution. Paired samples were compared by Wilcoxon test. Depending on whether the data were normally distributed, comparisons of three or more groups were conducted using either the Kruskal–Wallis test or an ANOVA with Tukey's multiple comparisons test. For parametric data analysis, Pearson's *r* was used to examine correlation. Statistical significance was determined using a two-tailed *P* value of < 0.05. Graphs and statistical analyses were generated using GraphPad Prism 6.0 (GraphPad Software). Materials and procedures in this study are described in detail in the supplemental information.

Results

Exhausted $CD8^+$T-cell subsets with distinct clinical characteristics, phenotypes, and functions

Additional file 2: Table. S1 summarizes the biochemical and clinical features observed in patients with T1D. Fasting glucose and HbA1c levels were higher in T1D patients. Total exhausted $CD8^+$ T cells and their subsets were analyzed by flow cytometry (Fig. 1A). In patients with T1D, both total exhausted $CD8^+$ T cells ($CD44^+PD\text{-}1^+$) and TEX cells ($CD8^+CD44^+PD\text{-}1^+Slamf6^-TIM\text{-}3^+$) were significantly reduced ($P = 0.003$; $P < 0.0001$; Fig. 1B). However, T1D patients exhibited a higher frequency of TPEX cells ($CD8^+CD44^+PD\text{-}1^+LSlamf6^+TIM\text{-}3^-$) compared to healthy controls ($P < 0.0001$; Fig. 1B). Moreover, total exhausted $CD8^+$ T cells in T1D exhibited markedly reduced secretion of IL-2 (Additional file 3: Fig. S1A). In contrast, TPEX cells demonstrated a significantly increased production of IFN-γ and TNF-α, likely reflecting their combined effector function and exhausted phenotype ($P = 0.0005$; $P = 0.0075$; Fig. 1C). Both subsets of exhausted $CD8^+$ T cells exhibited reduced IL-2 secretion in T1D ($P = 0.0296$; $P < 0.0001$; Fig. 1C,D). We compared the levels of cytokines secreted by the two subsets of exhausted $CD8^+$ T cells in T1D and found that significantly lower levels of cytokines secreted by TEX cells, which is in line with results from previous studies [27] (Additional file 3: Fig. S1B). TPEX cells exhibited a stronger proliferative capacity in T1D patients than in healthy controls ($P = 0.0002$; Fig. 1E). However, no significant difference in the proliferative capacity of TEX cells was found between T1D patients and healthy controls (Fig. 1E). Ki67 levels were higher in both TPEX and TEX cells in T1D patients ($P = 0.0061$; $P = 0.0052$; Fig. 1F). CD69 levels in TEX cells were significantly lower in T1D patients ($P = 0.0005$; Fig. 1G). The results suggest that TPEX cells have a higher proliferative capacity in T1D patients than in healthy controls. We further evaluated the cytotoxic function of both subsets and found that TPEX cells exhibited weaker cytotoxicity in T1D patients ($P = 0.0065$; Fig. 1H). No significant difference was observed in granzyme B secretion by TEX cells between T1D patients and healthy controls, as illustrated in Fig. 1I. Additionally, there was a significant increase in the total apoptosis proportion of the two subsets in T1D patients ($P = 0.0002$; $P = 0.0035$; Fig. 1J). Therefore, exhausted $CD8^+$ T cells from type 1 diabetic patients have potentially a higher proliferative capacity and are more prone to apoptosis.

Next, we explored the associations between T1D clinical characteristics and exhausted $CD8^+$ T cells. We noted a significant rise in the frequency of total exhausted $CD8^+$ T cells in individuals with a disease duration exceeding 2 years (Additional file 3: Fig. S1C). In contrast, no notable differences were observed in the frequencies of TPEX and TEX cells between patients diagnosed within 2 years and those with a longer disease duration (Additional file 3: Fig. S1C). Among the ten patients monitored over a 6-month period, the overall frequency of exhausted $CD8^+$ T cells remained stable as the disease progressed (Additional

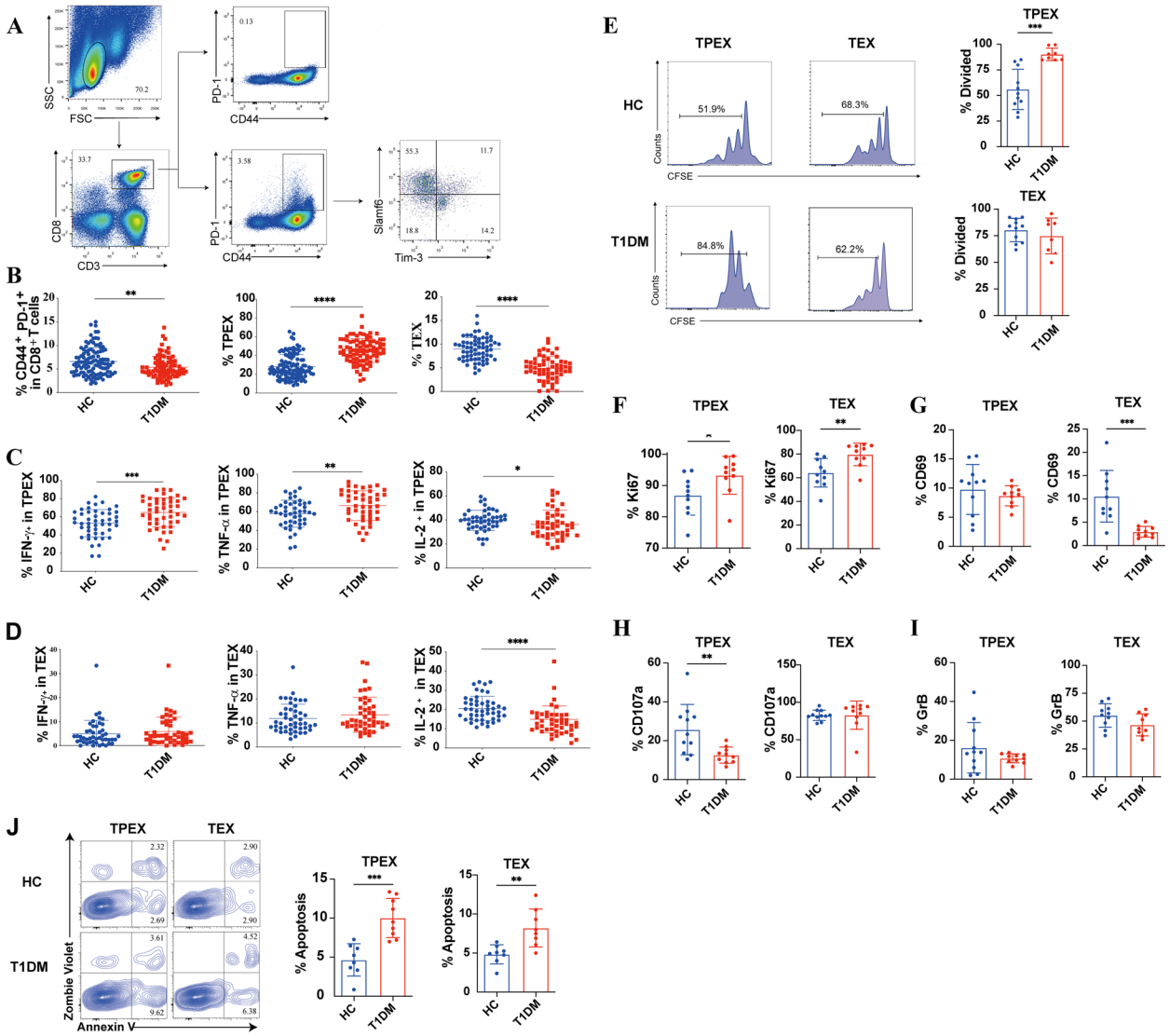

Fig. 1 Characterization of circulating exhausted CD8$^+$ T cells subsets in T1D. **A** Representative flow cytometry plots showing the gating strategy for exhausted CD8$^+$ T cells subsets. **B** The frequencies of total exhausted CD8$^+$ T cells and their subsets in patients with T1D ($n=87$) and healthy controls ($n=111$). **C, D** The expression of IFN-γ, TNF-α, and IL-2 in TPEX and TEX was measured by flow cytometry 5 h after stimulation with PMA, ionomycin, and brefeldin A ($n=45$) in patients with T1D and healthy controls ($n=47$). **E** Proliferation (assessed by CFSE dilution) of exhausted CD8$^+$ T cells subsets plated for 3 days with CFSE-labeled plus anti-CD3 and anti-CD28 in T1D patients ($n=8$) and healthy controls ($n=23$). **F–I** Ki67, CD69, CD107, and GrB expression from exhausted CD8$^+$ T cells subsets in T1D patients ($n=10$) and healthy controls ($n=11$). **J** The frequency of apoptotic cells within the exhausted CD8$^+$ T cell subsets was assessed in both healthy controls ($n=11$) and T1D patients ($n=10$). $^*P<0.05$; $^{**}P<0.01$; $^{***}P<0.001$; $^{****}P<0.0001$. Two-sided Student's *t* test (**B,C**). Mann–Whitney test (**D–J**). FSC, forward-scatter; SSC, side-scatter; HC, healthy controls

file 3: Fig. S1D). However, after 6 months of follow-up, a significant reduction in TPEX cells was observed, while the frequency of TEX cells increased in patients with T1D (Additional file 3: Fig. S1D). We classified patients with no detectable insulin secretion (C-peptide < 3.33 pmol/L) and a diagnosis within 4 years as rapidly progressing. Patients with C-peptide levels > 3.33 pmol/L and a diagnosis of 4 years or more were classified as slow progressors. Our findings indicated that TPEX cell numbers were significantly higher in T1D patients with slower disease progression (Additional file 3: Fig. S1E). Additionally, we noted a higher frequency of TEX cells in rapid progressors (Additional file 3: Fig. S1E).

Phenotypes and functions of exhausted CD8$^+$T-cell subsets in NOD mice

The kinetic change of exhausted CD8$^+$ T cells in the NOD mice was then examined. Only a minor rise in

the frequency of total exhausted CD8$^+$ T cells was observed in the lymph nodes and spleen until the age of 15 weeks (Fig. 2A). However, following significant destruction of islet cells and a substantial release of autoantigens at 25 weeks of age, the frequency of total exhausted CD8$^+$ T cells decreased rapidly (Fig. 2A). TPEX cell alterations were similar to those of total exhausted CD8$^+$ T cells (Fig. 2A). In contrast, the frequency of TEX cells exhibited a slight increase over time (Fig. 2A). Although the frequency of total exhausted CD8$^+$ T cells was elevated in diabetic mice compared to nondiabetic controls, the difference did not reach statistical significance (Fig. 2B). Notably, the frequency of TPEX cells was significantly higher in diabetic NOD mice ($P=0.0317$), while no significant difference was observed in the frequency of TEX cells between the two groups (Fig. 2B). We further investigated the expression of exhausted CD8$^+$ T cells and their subsets in NY8.3 mice with rapid disease progression and in NOD mice with relatively slow disease progression. Our findings revealed a significantly higher expression of total exhausted CD8$^+$ T cells in NY8.3 mice compared to age-matched NOD

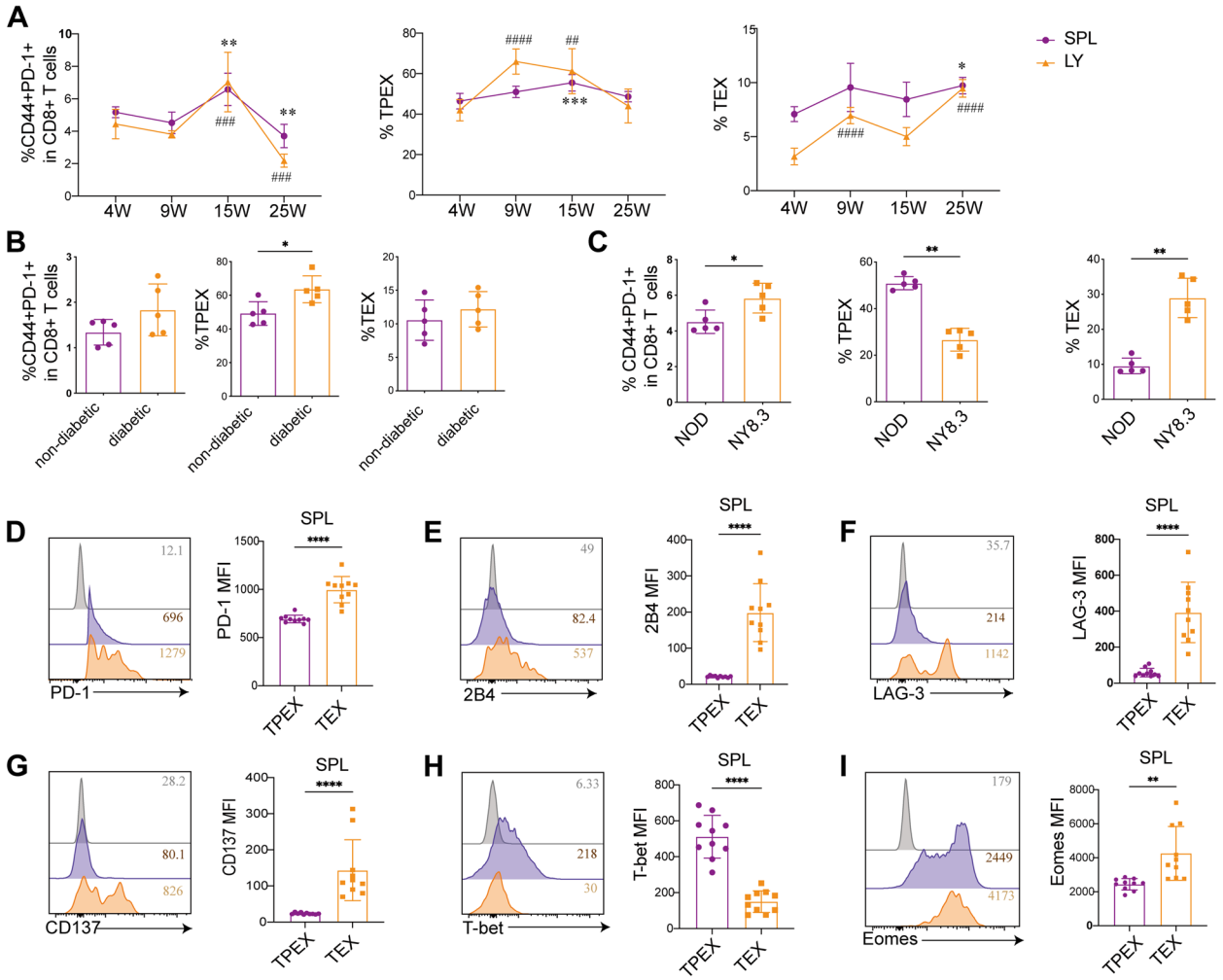

Fig. 2 Quantification, functionality, and co-receptor expression of exhausted CD8$^+$ T cells and their subsets in NOD mice. **A** The frequencies of exhausted CD8$^+$ T cells and their subsets were assessed in the draining lymph nodes and spleen of mice at ages 4, 9, 15, and 25 weeks ($n=6$/group). **B** The frequencies of exhausted CD8$^+$ T cells and their subsets in diabetic and non-diabetic NOD mice ($n=5$/group). **C** The frequencies of exhausted CD8$^+$ T cells and their subsets in the rapidly progressing non-diabetic NY8.3 mice and the slowly progressing non-diabetic NOD mice ages 10 weeks ($n=5$/group). **D–G** Co-expression of immune checkpoints on exhausted CD8$^+$ T subsets in NOD mice aged 8–13 weeks ($n=10$/group). **H, I** T-bet and Eomes on exhausted CD8$^+$ T subsets in NOD mice aged 8–13 weeks ($n=10$/group). MFI, mean fluorescence intensity. **A** * $P<0.05$; ** $P<0.01$; ***0.001. ## $P<0.01$; ### $P<0.001$; #### $P<0.0001$. * compare with 4 weeks in spleen; # compare with 4 weeks in lymph node. **B–I** *$P<0.05$; **$P<0.01$; ****$P<0.0001$. One-way ANOVA, Tukey's multiple comparisons test (**A**); Mann–Whitney test (**B–I**). Data are cumulative results from at least two independent experiments

mice ($P=0.0243$; Fig. 2C). Conversely, the expression of TPEX cells was notably elevated in the slowly progressing NOD mice, aligning with observations in T1D patients ($P<0.0001$; Fig. 2C). NY8.3 mice demonstrated a markedly increased frequency of TEX cells when compared to NOD mice ($P<0.0001$; Fig. 2C).

We determined the expression of both inhibitory and activated receptors. Compared to effector $CD8^+(CD44^+PD\text{-}1^-)$ T cells, total exhausted $CD8^+$ T cells exhibited significantly higher expression of 2B4, LAG3, and CD137 (Additional file 3: Fig. S2A, C, E). We next confirmed that TEX cells also enhanced the expression of PD-1, 2B4, LAG-3, and CD137 ($P<0.0001$; $P<0.000$; $P<0.0001$; $P<0.0001$; Fig. 2D–G) (Additional file 3: Fig. S2B, D, F). Cells with high PD-1 levels showed elevated CD137 expression, which may be a result of recent antigen contacts [54]. Our results suggested that TCR triggering could be the cause of the TEX cell phenotype. Previous research has showed that high Eomes expression might positively regulate exhaustion [55]. Compared to effector $CD8^+$ T cells, total exhausted $CD8^+$ T cells exhibited higher levels of Eomes and T-bet (Additional file 3: Fig. S2G-H). In the spleen, TEX cells produced more Eomes ($P=0.0023$), but TPEX cells expressed more T-bet ($P<0.0001$), as seen in Figs. 2 H and I. However, in the lymph nodes, TEX cells expressed more T-bet and Eomes (Additional file 3: Fig. S2I).

The unique transcriptional characteristics of exhausted $CD8^+$T-cell subsets in NOD mice

We further characterized exhausted $CD8^+$ T cells by analyzing RNAseq data. The data filtered by principal component analysis of variance (ANOVA) clearly separated the three groups (Fig. 3A). Comparative analysis of NOD mice revealed differential gene expression between TEX and TEFF cells, TPEX and TEFF cells, and TPEX and TEX cells, with 5899, 1112, and 5202 genes, showing significant differences, respectively. The overlap among the differentially expressed genes from each comparison is illustrated in Fig. 3B. Furthermore, an ANOVA analysis of 34,745 genes with above-background expression levels revealed 337 genes that were differentially expressed across TPEX, TEX, and TEFF cells (Fig. 3C). The biological processes that were significantly altered in TPEX, TEX, and TEFF cells were subsequently identified using pathway enrichment analysis (Fig. 3D). Hierarchical clustering analysis identified ten gene clusters with different expression levels among TPEX, TEFF, and TEX cells (Fig. 3E). We found that differential genes in these cells were primarily enriched in pathways associated with apoptosis, metabolism, cell cycle regulation, chemokines, and cytokine-cytokine receptor interactions (Fig. 3E). Additionally, by comparing the two exhausted $CD8^+$ T-cell subsets, we were able to identify a group of 4809 genes that showed differential expression (Fig. 3F). The two subsets differed mainly in cell survival, immune cell signaling pathways, and metabolism-related signaling pathways according to KEGG enrichment analysis (Fig. 3G). The mechanisms driving T-cell exhaustion in T1D were further examined using gene-set enrichment analysis (GSEA). TPEX cells upregulated the T-cell receptor signaling ($P<0.000$), cell cycle ($P<0.000$), and DNA replication signatures ($P<0.000$), while TEX upregulated the mitochondrial dysfunction gene signature ($P<0.000$) (Fig. 3H).

The transcriptional profiling data revealed an enrichment of genes associated with cytokine-cytokine receptor interaction signaling in TEX cells. Further study revealed that TPEX cells had much greater levels of IL-2Ra, IL-2Rb, and IL-2Rg expression ($P=0.0074$, $P=0.0004$, $P=0.0004$) whereas TEX cells had significantly higher levels of IL-10R expression ($P=0.0333$) (Fig. 4A). First, we evaluated if TPEX cells could produce cytokines again and exhibit less PD-1 when expanded in vitro with IL-2 (Fig. 4B). The TPEX cells showed a lower expression of PD-1 ($P=0.0235$) and failed to secrete substantial amounts of IFN-γ and TNF-α ($P=0.0286$), which was consistent with the phenotype of T1D patients (Fig. 4C,D). IL-2-treated TPEX cells rapidly re-expressed more PD-1-negative effector T cells ($P=0.0300$), whereas no substantial effect on controls was observed (Fig. 4E). When TPEX cells were exposed to IL-10, no substantial effect was observed on PD-1 expression and IFN-γ secretion (Fig. 4F–H). The level of TNF-α was significantly decreased ($P=0.0248$) (Fig. 4H). TPEX cells did not differentiate into TEX cells (Fig. 4I). Additionally, we

(See figure on next page.)

Fig. 3 The gene transcription profile for NOD mouse exhausted $CD8^+$ T cells and their subsets. $n=3$ biologically independent samples. **A** Principal component analysis for sorted exhausted CD8.$^+$ T cells and their subsets from NOD mice. **B** Genes showing significant regulation between the three subsets. Significance was defined as log2 fold change ≥ 1 and Benjamini–Hochberg FDR < 0.01. **C** Heatmap of RNA-seq data for TEFF, TPEX, and TEX subsets. **D** Kyoto Encyclopedia of Genes and Genomes (KEGG) enriched in all differential genes in TEFF, TPEX, and TEX subsets. **E** Key biological processes are either up- or downregulated in specific clusters. **F** Heatmap of RNA-seq data for TPEX and TEX subsets. **G** KEGG enriched in all differential genes in TPEX and TEX subsets. **H** Published data sets from subsets of exhausted T lymphocytes in NOD mice using gene set enrichment analysis (GSEA). NES, normalized enrichment score. FDR, false discovery rate. One-way ANOVA (**B–D**); Mann–Whitney test (**F**)

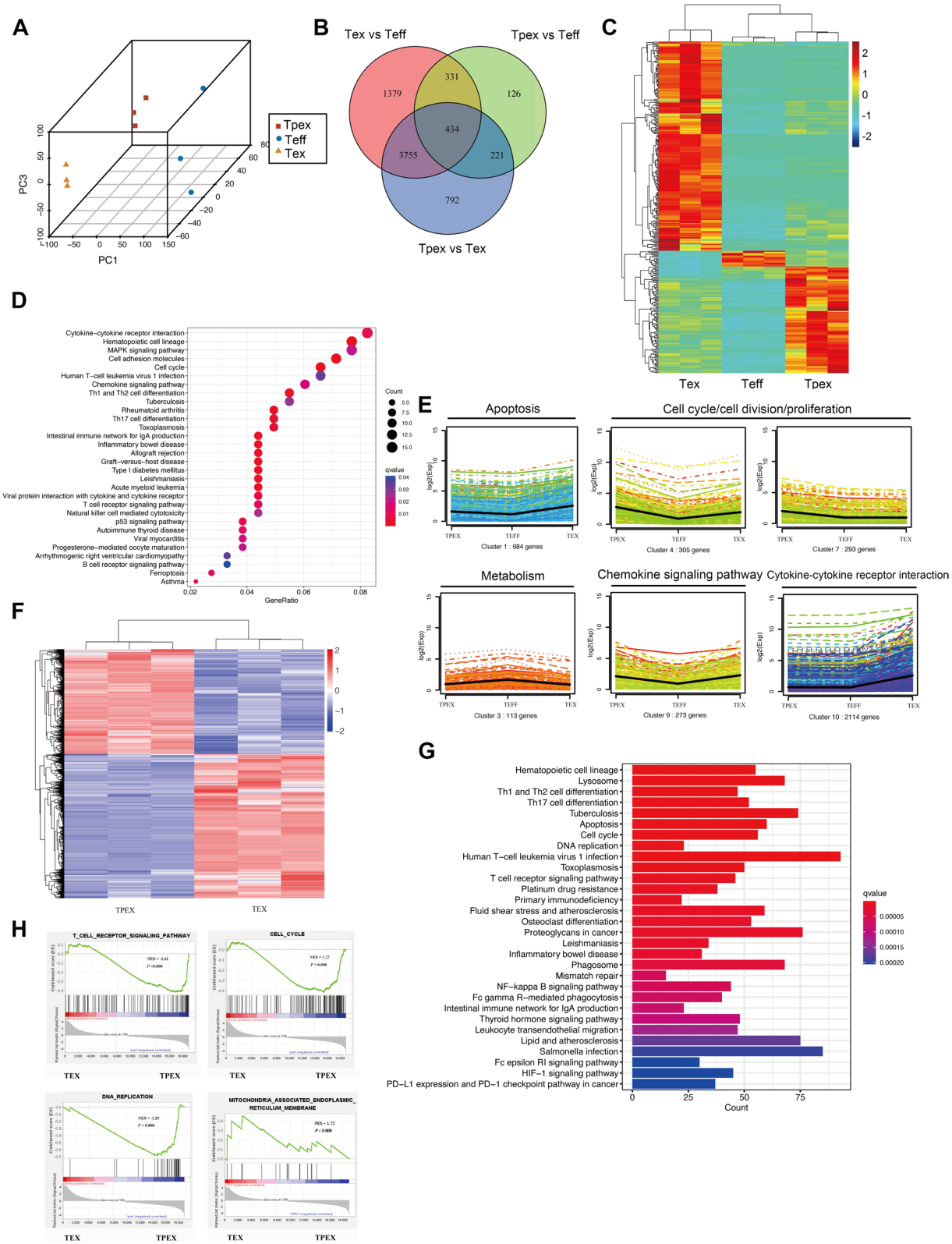

Fig. 3 (See legend on previous page.)

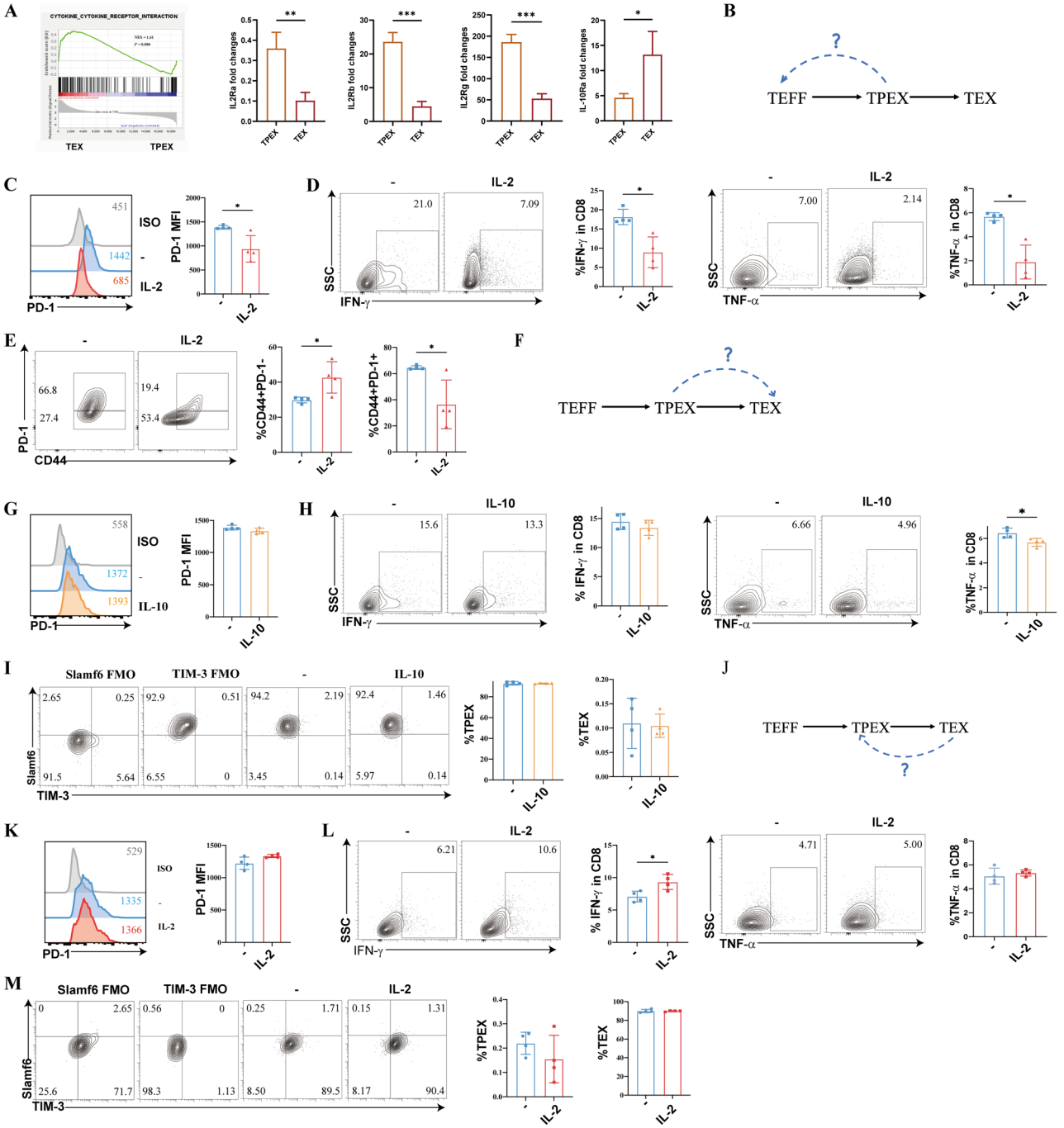

Fig. 4 A fixed state of malfunction is exhibited by exhausted CD8$^+$ T cell subsets ($n=4$/group). **A** GSEA examining the enrichment of genes associated with cytokine-cytokine receptor interaction signaling in exhausted CD8$^+$ T cell subsets in NOD mice. Expression of the cytokine-cytokine-receptor genes at the mRNA level in the exhausted CD8$^+$ T cell subsets. **B** Diagram showing the experimental design for the conversion of TPEX cells into TEFF cells. **C** Expression of PD-1 in IL-2 expanded sorted TPEX cells. **D** IFN-γ and TNF-α expression in IL-2 expanded sorted TPEX cells. **E** The proportion of exhausted CD8$^+$ T cells that are CD44$^+$PD-1$^-$ and CD44$^+$PD-1$^+$ in IL-2 expanded sorted TPEX cells. **F** Diagram showing the experimental design for the conversion of TPEX cells into TEX cells. **G** PD-1 expression in sorted TPEX cells following IL-2 removal and short exposure to IL-10. **H** IFN-γ and TNF-α expression in sorted TPEX cells following IL-2 removal and short exposure to IL-10. **I** The percentage of TEX cells and TPEX cells in sorted TPEX cells following IL-2 removal and short exposure to IL-10. **J** Diagram showing the experimental design for the conversion of TEX cells into TPEX cells. **K** Expression of PD-1 in IL-2 expanded sorted TEX cells. **L** IFN-γ and TNF-α expression in IL-2 expanded sorted TEX cells. **M** The percentage of TPEX and TEX cells in IL-2 expanded sorted TEX cells. *$P<0.05$; **$P<0.01$; ***$P<0.001$. Mann–Whitney test. Data are cumulative results from two independent experiments

investigated whether adding IL-2 to TEX cells in vitro might decrease PD-1 expression and restore cytokine production (Fig. 4J). Following treatment with IL-2, PD-1 expression remained unchanged (Fig. 4K). TEX cells did not release significant amounts of TNF-α; however, there was an increase in IL-2, leading to enhanced IFN-γ production ($P=0.0194$) (Fig. 4L). Furthermore, Fig. 4M shows that TEX cells did not differentiate into TPEX cells. These results imply that TPEX cells recovered their ability to perform effector functions, but they were not affected by immune-suppressive substances like IL-10. IL-2 could make it more difficult to reinvigorate TEX cells.

Exhausted CD8$^+$T-cell subsets displayed unique TCR reactivity and profound alterations in metabolism

The analysis of pathways involved in TPEX cells and TEX cells from NOD mice revealed a significant enrichment of genes associated with the peptide-binding pathway (Fig. 5A). The TPEX cells exhibited a more varied TCR repertoire than the TEX cells, according to the examination of TCR repertoires (Fig. 5B). The abundance of these clones was higher in TEX cells compared to TPEX cells (Fig. 5C). TPEX cells had a higher number of clonotypes, making up the most dominant 10% of repertoires (Fig. 5D). Additionally, we used the Chao1 estimator of richness, which quantifies the number of distinct TCR specificities, to estimate diversity. In the analysis of the TCRβ repertoire, the Chao1 index was decreased in TEX cells compared to TPEX cells (Fig. 5E). Interestingly, we observed that $IGRP_{206–214}$ antigen-specific stimulation induced more total exhausted CD8$^+$ T cells than anti-CD3 stimulation. $IGRP_{206–214}$ stimulation resulted in more TEX cells than anti-CD3 stimulation, while anti-CD3 stimulation led to an increase in TPEX cells (Fig. 5F). Our results suggest that antigen-specific immunotherapy may induce more durable immune tolerance by increasing both total exhausted CD8$^+$ T cells and TEX cells.

Recent findings from murine tumor models indicate that when exhausted T cells infiltrate the tumor microenvironment (TME), they undergo substantial metabolic changes, leading to metabolic dysfunction [56]. Strikingly, glucose uptake was significantly decreased in total exhausted CD8$^+$ T cells compared to effector CD8$^+$ T cells (Additional file 3: Fig. S3A). TPEX cells in lymph nodes exhibited a significantly increase in glucose uptake compared to TEX cells (Additional file 3: Fig. S3A). However, there was no significant difference in glucose uptake between the two subsets in the spleen (Fig. 5G). The lipid content (Bodipy 493) was significantly different between exhausted and effector CD8$^+$ T cells, but not between the two subsets of exhausted CD8$^+$ T cells (Additional file 3: Fig. S3B, Fig. 5H). MitoTracker green (MTG) labeling revealed that TEX cells and total exhausted CD8$^+$ T cells had a greater mitochondrial mass ($P<0.0001$) (Additional file 3: Fig. S3C, Fig. 5I). In the lymph nodes and spleen, TEX cells displayed a markedly decreased mitochondrial membrane potential (MTR) ($P=0.0029$), which persisted even after MTR was normalized to the mitochondrial mass ($P<0.0001$) (MTR/MTG ratio), suggesting persistent mitochondrial dysfunction (Additional file 3: Fig. S3D-E, Fig. 5I). TEX cells expressed higher levels of the scavenger receptor CD36, which is essential for the uptake of fatty acids ($P<0.0001$) (Fig. 5J, Additional file 3: Fig. S2J-K).

Transmission electron microscopy confirmed that although TEX cells had more mitochondria ($P<0.0001$), these mitochondria had undergone significant morphological alterations, including fewer cristae ($P<0.0001$) and a tendency toward shorter cristae ($P<0.0001$) (Fig. 5K). TPEX cells and total exhausted CD8$^+$ T cells in the lymph nodes expressed more cytochrome c proteins (Additional file 3: Fig. S3F). No significant differences were observed in CytoC protein levels between exhausted CD8$^+$ T cells and their subsets in the spleens (Additional file 3: Fig. S3F, Fig. 5L). We found that exhausted CD8$^+$ T lymphocytes in the lymph nodes and spleen did not exhibit a significant increase in ATP5O (Fig. 5M, Additional file 3: Fig. S3G). Moreover, we examined the level of mitochondrial ROS in exhausted CD8$^+$ T cells. Both total exhausted CD8$^+$ T cells and TPEX cells exhibited a much higher concentration of mitochondrial superoxide ($P<0.0001$)(Additional file 3: Fig. S3H, Fig. 5N).

Lrrk2 plays a role to alter the phosphorylation of Drp1-Ser637 and initiates mitochondrial fission

T-cell exhaustion is associated with mitochondrial dysfunction [57]. In our analysis, we observed a significant enrichment of genes associated with the mitochondria-associated endoplasmic reticulum membranes (MAMs) pathway (Fig. 3H). MAMs are involved in various cellular processes, including ER stress, mitophagy, mitochondrial dynamics, and Ca^{2+} exchange [58, 59]. The flux of repeated fusion and fission events of the organelles balances the dynamic networks formed by mitochondria in the cell [60]. Dynamin-related protein 1 (Drp1) is a crucial mediator of mitochondrial fission and maintaining integrity of the mitochondrial network [61]. We screened the gene expression associated with the formation of MAMs in RNA-seq. The mRNA expression of dynamin 1 like (*Dnm1l*) was not increased significantly in TPEX cells compared with TEX cells (Fig. 6A). We predicted a primary interaction network between *Dnm1l* and leucine-rich repeat kinase 2 (*Lrrk2*) using the STRING database (Fig. 6B). The

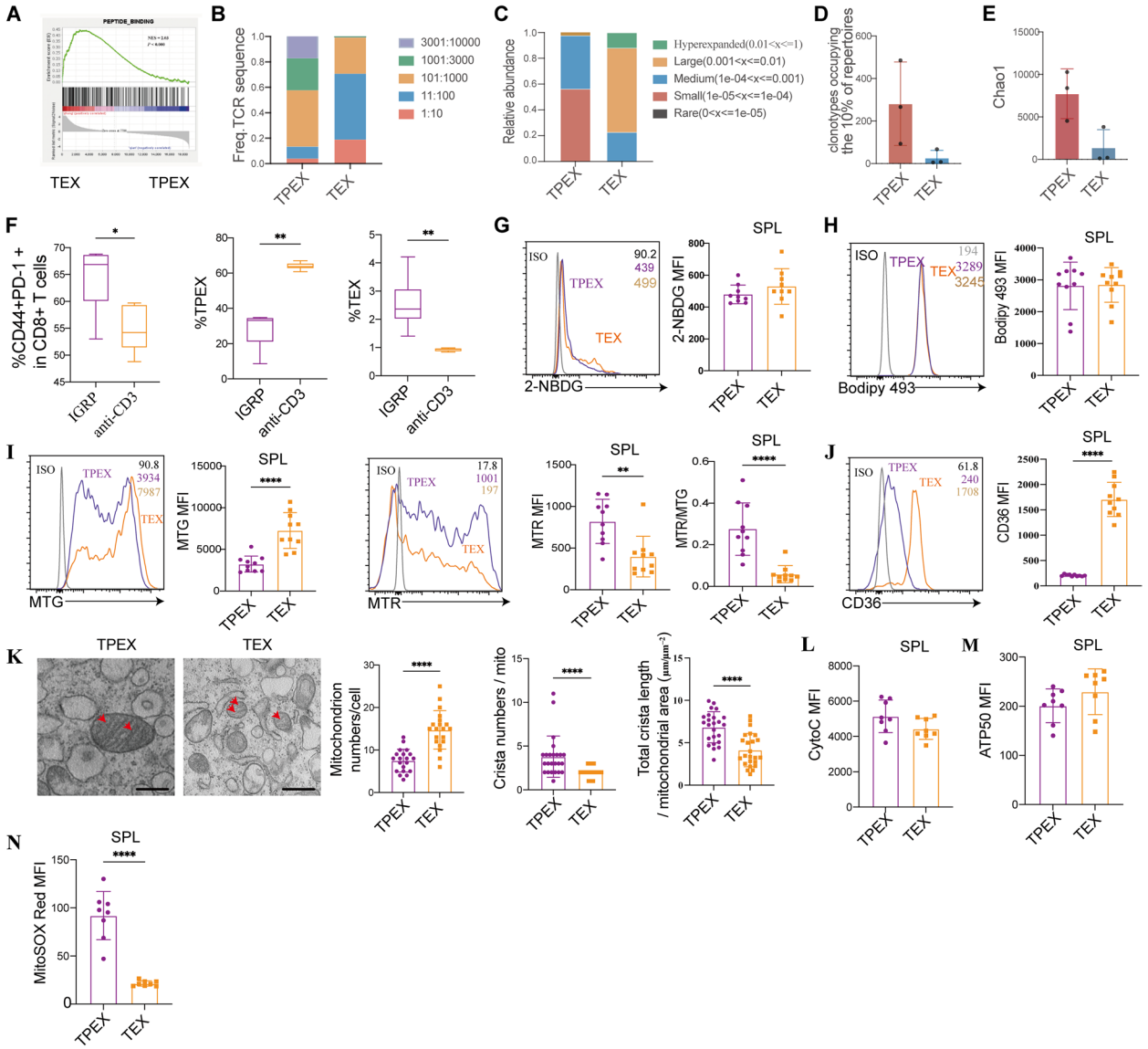

Fig. 5 Alterations in TCR repertoires, glucose, fatty acids, and mitochondrial metabolism in exhausted CD8$^+$ T cell subsets. **A** GSEA examining the enrichment of genes associated with peptide-binding signaling in exhausted CD8$^+$ T cell subsets in NOD mice. **B** TCR Diversity within the TPEX and TEX cells in NOD mice. Data from three samples of five mice each mixed are shown. **C** The proportions of the hype expanded frequent TCR β clonotype, the large frequent, the medium frequent, the small frequent, and the rare clonotypes are shown for TPEX and TEX populations. **D** The clonotypes occupying the most dominant 10% of repertoire within the TPEX and TEX cells. **E** Boxplot of Chao1 indices for TPEX and TEX cells. **F** CD8$^+$ T cells isolated from NY8.3 mice and treated for 72 h with either IGRP$_{206–214}$ (10 μmol/L) or CD3 (1 μg/ml) and CD28 (2 μg/ml) ($n=5$/group). Total exhausted CD8$^+$ T cells, TPEX, and TEX cells were measured by flow cytometry after stimulation. **G** 2-NBDG ($n=9$/group), **H** Bodipy 493 ($n=9$ / group), **I** MTG, MTR, and normalized ΔΨm (MTR/MTG ratio) ($n=10$/group), and **J** CD36 expression of TPEX and TEX populations in NOD mice ($n=10$/ group). **K** Electron micrographs showing the randomly chosen mitochondrial ultra-structures of sorted TPEX and TEX cells in NOD mice ($n=24$/ group). ImageJ was used to quantify the number of mitochondria per cell, the number of cristae within mitochondria, and the total cristae length normalized to the mitochondrial surface area. The analyzer and at least ten randomly chosen cells in each group were blinded to the identity of the samples. **L** Cytoc, **M** ATP5O, and **N** MitoSOX red expression of TPEX and TEX populations in NOD mice. *$P<0.05$, **$P<0.01$, ****$P<0.0001$. Mann–Whitney test (**D–N**). Scale bars, 500 μm. Data represent three independent experiments

expression of *Lrrk2* was low in TPEX cells but high in TEX cells ($P=0.0007$; Fig. 6A). Phosphorylation at two important serines has conflicting effects that quickly regulate Drp1 activity [62]. Drp1 activity is increased when serine 616 (Drp1-Ser616) is phosphorylated, and decreased when serine 637 (Drp1-Ser637) is phosphorylated. Therefore, we speculated that whether Lrrk2 can influence mitochondrial fission by regulating the

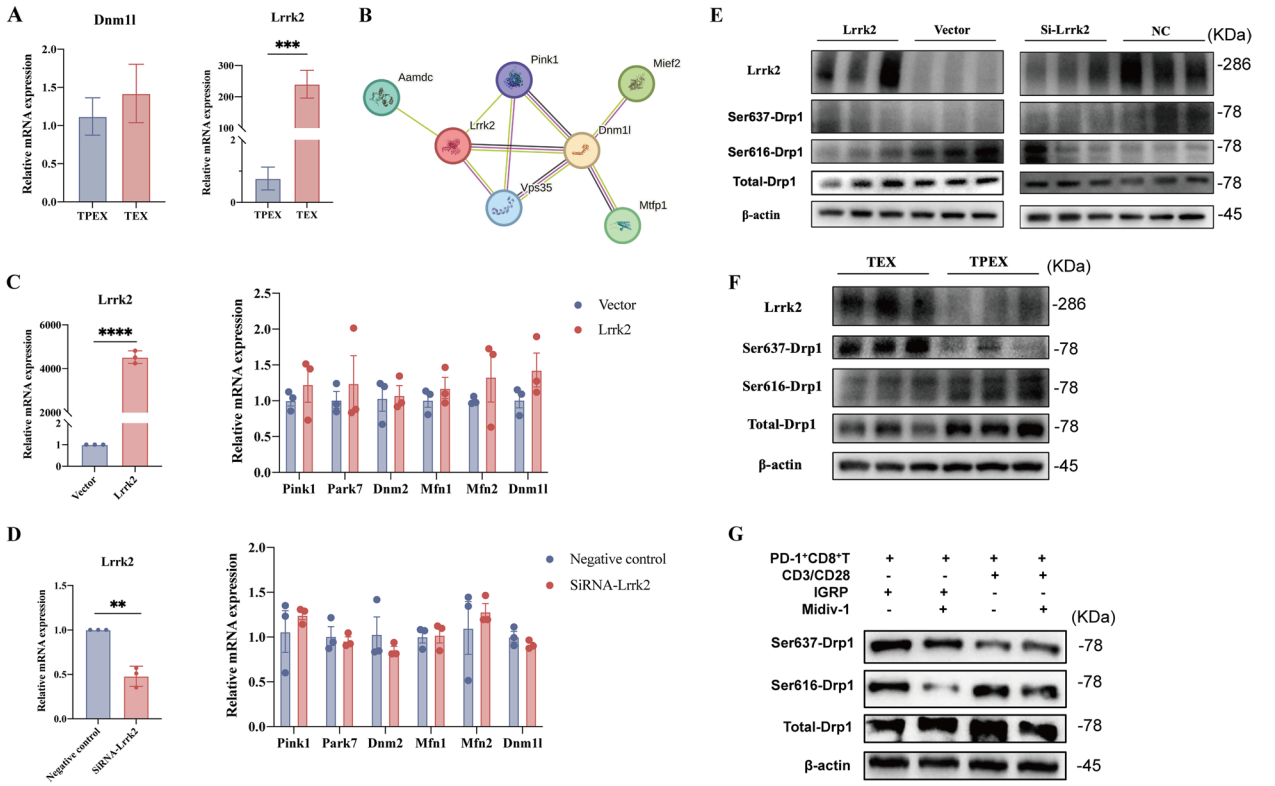

Fig. 6 Lrrk2 plays a role to alter the phosphorylation statu triggers mitochondrial fission ($n = 3$/group). **A** Sorted TPEX and TEX cells obtained from 16-week-old non-diabetic NOD mice were examined using qPCR to determine the expression of *Dnm1l* and *Lrrk2*. **B** Interaction network depicting between *Dnm1l* and *Lrrk2* using the STRING database. **C** The *Lrrk2* plasmid was used to transfect the 293 T cells. Cells were lysed for qPCR analyses. **D** The *Lrrk2* plasmid was used to transfect the 293 T cells, followed by knockdown. Cells were lysed for qPCR analyses. **E** The 293 T cells were transfected with *Lrrk2* plasmid or were transfected with *Lrrk2* plasmid, followed by knockdown. Cells were lysed for immunoblotting analyses. **F** Western blot analysis was used to determine the protein expression in sorted TPEX and TEX cells that were separated from 8-week-old NY8.3 mice. **G** Sorted PD-1^{+}CD8^{+} T cells in NY8.3 mice aged 6–8 weeks, stimulated them with anti-CD3 and anti-CD28 or $IGRP_{206–214}$ for 3 days, with or without the Midiv-1. Collected the cells and analyzed using Western blotting. ***$P < 0.001$, ****$P < 0.0001$. Mann–Whitney test (**A**, **C,D**). Data represent two independent experiments

phosphorylation of Drp1. The expression of MAM-associated genes, including Dnm1l, did not change in response to either overexpression of the Lrrk2 gene ($P < 0.0001$) or a subsequent knockdown of the over-expressed Lrrk2 ($P = 0.0013$) in 293 T cells (Fig. 6C,D). Increased expression of Lrrk2 can promote the phosphorylation of Drp1-Ser637 while inhibiting the phosphorylation of Drp1-Ser616 (Fig. 6E). Additionally, following Lrrk2 overexpression and subsequent knockdown, the phosphorylation of Drp1-Ser616 was elevated compared to the control group, but the phosphorylation of Drp1-Ser637 was significantly reduced in 293 T cells (Fig. 6E). Furthermore, we isolated TPEX cells and TEX cells from NY8.3 mice. In contrast to TPEX cells, TEX cells showed reduced phosphorylation at Ser616 and elevated phosphorylation at the Ser637 site of Drp1, as well as increased expression of Lrrk2 (Fig. 6F). Therefore, phosphorylation of Drp1 may regulate the interconversion of two subsets of exhausted T cells. Mdivi-1, a mitochondrial division inhibitor, mainly prevented Drp1 from functioning by inhibiting the phosphorylation of Drp1 at the Ser616 site [63]. In the anti-CD3 stimulation group, treatment with Mdivi-1 led to a decrease in DRP1 phosphorylation at Ser616, accompanied by a significant increase in phosphorylation at Ser637. Conversely, in the $IGRP_{206–214}$ stimulation group, Mdivi-1 reduced DRP1 phosphorylation at Ser616 without causing a notable change in phosphorylation at Ser637 (Fig. 6G).

It has been demonstrated that using mitochondrial uncouplers to induce mitochondrial damage in addition to TCR stimulation significantly increases the proportion of depolarized mitochondria [56]. Treatment with Mdivi-1 with or without oligomycin and antimycin A (OA) supported the notion that it promotes the development of total exhausted CD8^{+} T-cells in response to both anti-CD3 and $IGRP_{206–214}$ stimulation (Additional file 3: Fig. S4A). Furthermore, OA and Mdivi-1 treatment

effectively increased the formation of TEX cells under both $IGRP_{206–214}$ and anti-CD3 stimulation (Additional file 3: Fig. S4B). Additionally, our results show that oligomycin and antimycin A together with Mdivi-1, decreased effector cytokines in TEX cells but not in TPEX cells (Additional file 3: Fig. S4C-D).

Blockade of Mitochondrial fission improved the immunotherapy efficacy of anti-CD3 mAb by inducing more TEX cells

It has been reported that treatment with anti-CD3 mAb can delay the progression of β-cell dysfunction in patients with recent-onset clinical T1D [32]. Our findings indicate that antigen-specific immunotherapy may promote longer-lasting immune tolerance by boosting the presence of total exhausted $CD8^+$ T cells and TEX cells. We next conducted experiments to evaluate the effects of $IGRP_{206–214}$ and anti-CD3mAb on the proliferation of exhausted $CD8^+$ T-cell subsets. In NOD SCID mice, we adoptively transferred effector $CD8^+$ T cells derived from NY8.3 mice (Fig. 7A). On day 5, the group treated with $IGRP_{206–214}$ exhibited a significantly higher proportion of total $CD8^+$ T cell ($P=0.0013$) (Fig. 7B). The $IGRP_{206–214}$-treated group induced more TEX cells ($P=0.0022$) while the anti-CD3 mAb-treated group mainly induced TPEX cells ($P=0.0043$) (Fig. 7B). On day 15, the $IGRP_{206–214}$-treated group had a higher proportion of TEX cells ($P<0.0001$) and a lower proportion of TPEX cells ($P<0.0001$) compared to the anti-CD3 mAb-treated group (Fig. 7C). Additionally, we observed the immunotherapy effects by treating NY8.3 mice with anti-CD3mAb and $IGRP_{206–214}$ (Fig. 7D). Compared to the NY8.3 mice treated with anti-CD3mAb, those treated with $IGRP_{206–214}$ significantly delayed the onset of diabetes ($P=0.0284$) (Fig. 7E) and improved insulitis (Fig. 7F). One week after treatment, $CD8^+$ T cells were separated and single-cell RNA sequencing (scRNA-seq) was used to observe whether the subsets of exhausted T cells were different.

Single-cell transcriptomic landscape of anti-CD3 mAb and IGRP immunotherapy

By applying uniform manifold approximation and projection (UMAP) for unsupervised clustering, we identified six distinct T cell populations. The group treated with anti-CD3 mAb mainly produced more TPEX cells, naïve T cells, and a small amount of TEX cells, while the $IGRP_{206–214}$-treated group was primarily composed of naïve T cells, TEX cells, and TEFF cells (Fig. 8A). In the anti-CD3 mAb-treated group, TPEX cells were identified by a combination of memory-related molecules (Ccr7, Id3, Tcf7, Slamf6, and Sell) and exhaustion marker (Pdcd1). In contrast, the $IGRP_{206–214}$-treated group showed a progressive upregulation of terminal exhaustion markers, including Pdcd1, Lag3, Nr4a2, and Havcr2 (encoding for Tim-3) (Fig. 8B). The activation, signal transduction, and proliferation functions of TCR in $CD8^+$ T cells persisted at a high level in naïve T cells and TPEX cells following anti-CD3 mAb treatment; however, these activities were dramatically reduced in the $IGRP_{206–214}$ group (Fig. 8C). In the $IGRP_{206–214}$-treated group, although the T-cell signaling pathway was predominantly expressed in TEFF cells, these cells were notably enriched in apoptosis and immune negative regulation signaling pathways, exhibiting a terminally differentiated T-cell state compared to the anti-CD3mAb-treated group (Additional file 3: Fig. S5A). Additionally, compared to the anti-CD3 mAb treatment group, the $IGRP_{206–214}$ group exhibited decreased activation, proliferation, migration, and co-stimulatory signals in various $CD8^+$ T cells, especially TEX cells, while endogenous and mitochondrial apoptotic signals were increased (Additional file 3: Fig. S5B). Monocle pseudotime analysis further corroborated the transitions from TPEX cells to the TEX cells in anti-CD3mAb treatment and $IGRP_{206–214}$ treatment (Fig. 8D). These might be the reason for achieving better overall therapeutic efficacy after $IGRP_{206–214}$ treatment. To illustrate the distinct subcellular interactions between groups treated with $IGRP_{206–214}$ and anti-CD3 mAb, we utilized the CellCall tool to investigate cell–cell communication. Contrary to the other two groups, the $IGRP_{206–214}$-treated group showed a significant decrease in intercellular crosstalk events (Fig. 8E). Compared to the anti-CD3mAb-treated group, the $IGRP_{206–214}$-treated group demonstrated a heightened interaction between TEX cells and other subsets (Additional file 3: Fig. S5C). We observed more inhibitory signal interactions between proliferative T cells, naïve T cells, and effector T cells with other cells in the $IGRP_{206–214}$-treated group than in the anti-CD3 mAb-treated group by visualizing ligand-receptor pairs involved in cell communication (THY1-ADGRE5, SELL-SELPLG, SPN-ICAM1, DHCR7-NR1H2 axis) (Fig. 8F). Additionally, within both the TPEX and TEX cell subsets, the $IGRP_{206–214}$-treated group showed elevated levels of inhibitory and apoptotic signals compared to the anti-CD3 mAb-treated group (Additional file 3: Fig. S5D).

Combination of anti-CD3 mAb and OA and Mdivi-1 (OAM) improves the immunotherapy outcomes in NOD mice

Therefore, we took advantage of OA and Mdivi-1 to determine whether combination anti-CD3mAb treatment could induce more TEX cells to delay the progression of autoimmune diabetes. We used $IGRP_{206–214}$ continuous stimulation to mimic the immune tolerance induced by antigen-specific stimulation in vitro. After

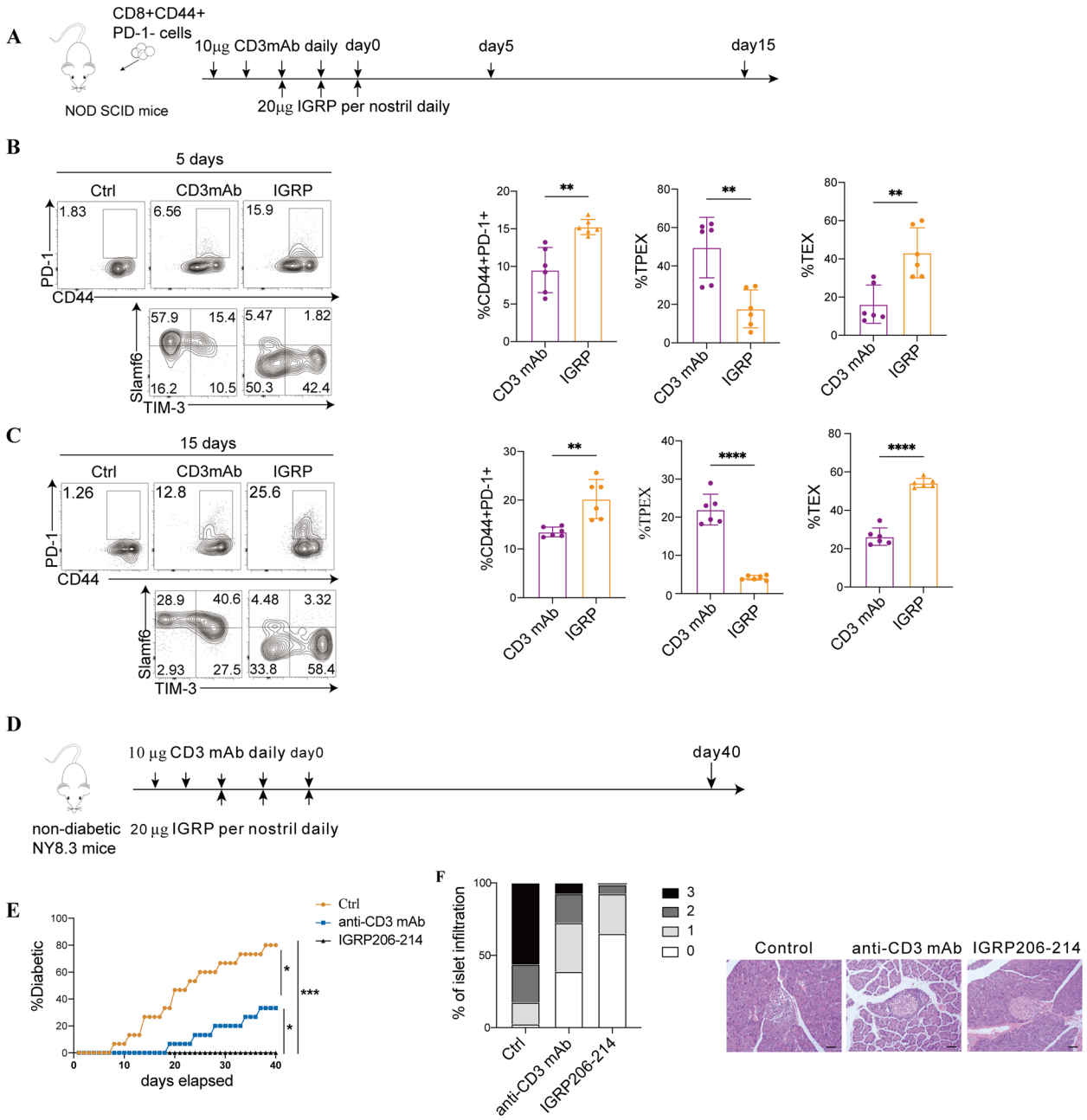

Fig. 7 Anti-CD3 mAb and IGRP therapy delays the autoimmune progression of T1D. **A** Experimental design for adoptive transfer studies. NOD SCID mice aged 8–10 weeks underwent an adoptive transfer of $CD8^+CD44^+PD\text{-}1^-$ T cells derived from NY8.3 mice aged 6–8 weeks. The recipient mice were treated with either 20 μg of $IGRP_{206–214}$ per nostril daily for three consecutive days or 10 μg of anti-CD3 monoclonal antibody (mAb) daily for 5 days. On days 5 and 15 post-treatment, the mice were sacrificed. Quantitative analysis and flow cytometry data of total exhausted $CD8^+$ T cells, as well as TPEX and TEX cells were collected on days 5 (**B**) ($n = 6$/group) and 15 (**C**) ($n = 6$/group). **D** Experimental design for NY8.3 mice immunotherapy studies. Four-week-old female NY8.3 mice ($n = 16$/group) were treated with 10 mg anti-CD3mAb or 20 μg $IGRP_{206–214}$ per nostril daily for 3 days. Mice were sacrificed at day 40 after treatment. **E** The prevalence of diabetes during the course of treatment in NY8.3 mice. **F** At day 40, the percentage of pancreatic islets exhibiting the specified histological scores in "non-diabetic" mice from **D** was measured. For insulitis, ten pieces per pancreas were blindly scored. (0 = no infiltrate, 1 = 0–25%, 2 = 25–75%, 3 ≥ 75%). White bars, 0; light grey bars, 1; dark grey bars, 2; black bars, 3. Representative pictures of the islets at day 40 "non-diabetic" mice from **D**. Mann–Whitney test (**B,C**); one-way ANOVA (**E**). Scale bars, 50 μm

overnight stimulation with $IGRP_{206–214}$ and IL-2, $CD8^+$ T cells derived from NY8.3 mice were separated and cleaned for analysis under five distinct circumstances. Cells were either cocultured with $IGRP_{206–214}$ and IL-2 ("continuous" activation) or expanded with IL-2 (activation) for 5 days. The media was changed frequently to avoid nutritional depletion. This post-activation expansion was carried out in the presence of OAM, anti-CD3 mAb, or a combination of both in round-bottomed plates (Additional file 3: Fig. S6A). Short-term or continuous $IGRP_{206–214}$ stimulation alone increased the production of total $CD8^+$exhausted T cells (Additional file 3: Fig. S6B-C). Combined continuous $IGRP_{206–214}$ stimulation and OAM did not result in an expansion of total exhausted T cells and their subsets compared with short stimulation or continuous $IGRP_{206–214}$ stimulation alone (Additional file 3: Fig. S6B-E). The combination of anti-CD3 mAb and OAM significantly increased total exhausted T cells and TEX cells compared with treatment with anti-CD3mAb alone (Additional file 3: Fig. S6B-E). The anti-CD3 mAb-treated group significantly inhibited the secretion of IFN-γ by TPEX cells with or without OAM, and had no effect on TNF-α in TPEX cells (Additional file 3: Fig. S6F-H). Anti-CD3 mAb treatment combined with OAM significantly limited polyfunctional cytokine production by TEX cells (Additional file 3: Fig. S6I-K).

To explore whether the blocking of mitochondrial fission promote the efficacy of anti-CD3 mAb immunotherapy, we administered $IGRP_{206–214,}$ anti-CD3 mAb and a combination of anti-CD3 mAb and OAM to 4-week-old female NY8.3 mice (Fig. 9A). By day 60 after treatment, all of the mice in the control group had developed diabetes (Fig. 9B). Conversely, during the course of treatment, none of the $IGRP_{206–214}$ groups had the onset of diabetes (Fig. 9B). Moreover, the combination of anti-CD3 mAb and OAM delayed diabetes and reduced islet inflammatory infiltration more significantly than anti-CD3 mAb alone ($P=0.0426$ (Fig. 9B,C). Compared to control mice, treatment with $IGRP_{206–214}$ led to a significant increase in the levels of both total $CD8^+$ T cells and TEX cells (Fig. 9D). Mice treated with anti-CD3 mAb and OAM exhibited a notably elevated number of total $CD8^+$ T cells ($P<0.0001$) and TEX cells ($P=0.0057$) compared to those receiving anti-CD3 mAb treatment alone (Fig. 9D). Next, we evaluated whether combining anti-CD3 mAb and OAM improved rates of hyperglycemia reversal in NY8.3 mice with new-onset diabetes (Fig. 9E). Conversely, continuous administration of anti-CD3 mAb alone normalized hyperglycemia in only 25.0% of mice (4/16). The combination of anti-CD3 mAb with OAM significantly increased the rate of hyperglycemia reversal, achieving a 75.0% success rate in treated NY8.3 mice ($n=12/16$) (Fig. 9F). In line with these results, the combination therapy showed less invasive insulitis than the anti-CD3 mAb alone (Fig. 9G). Thirty days after the commencement of treatment, the diabetic mice were euthanized, and their pancreata were examined using immunohistochemistry. Mice that were protected with combination therapy exhibited a significantly higher percentage of islets with reduced islet invasion compared to those protected with anti-CD3 monoclonal antibody (mAb) alone (Fig. 9G). Mice that underwent combination therapy displayed an elevated number of total $CD8^+$ exhausted T cells ($P=0.0212$) and TEX cells ($P<0.0001$) than animals that received anti-CD3 mAb alone, according to an analysis of lymph nodes from mice that were protected 30 days after starting of treatment (Fig. 9H,I). The proportion of TEX cells after combination therapy reached the level of TEX cells that showed $IGRP_{206–214}$-induced antigen-specific immune tolerance (Fig. 9H,I).

Combining anti-CD3 mAb with OAM induced T-cell exhaustion in PBMCs from T1D patients

We next investigated whether combining anti-CD3 mAb and OAM could be beneficial for immunotherapy in T1D patients. Notably, in T1D patients, TEX cells exhibited a greater mitochondrial mass compare to TPEX cells, as seen by MTG labeling ($P=0.0163$) (Fig. 10A,B). Even after ΔΨm was normalized to the mitochondrial mass (MTR/MTG ratio), TPEX cells displayed a significantly higher MTR (ΔΨm) compared to TEX cells in healthy controls ($P=0.0218$) (Fig. 10A,B). Additionally, in line with the findings in mice (Figure S4B-D), we found that OAM treatment enhanced the formation of total exhausted $CD8^+$ T cells ($P=0.0020$) and TEX cells ($P=0.0429$) decreased their production of effector

(See figure on next page.)

Fig. 8 Single-cell RNA sequencing was performed on $CD8^+$ T cells from Four-week-old NY8.3 mice 7 days after they were treated with anti-CD3mAb and $IGRP_{206–214}$. $n=2$ biologically independent samples. **A** tSNE clusters of cells from the scRNA-seq. **B** Dot plot examination of specific markers that reflect TPEX and TEX cell subsets; dot size and color intensity indicated the percentage of cells expressing the gene and the *z*-score mean expression, respectively. **C** Normalized signaling pathway expression projected onto UMAP clusters. **D** Slingshot analysis was used to predict developmental trajectories. Color-coding of cells was based on pseudotime. **E** Cellcell communication analysis by Cellcall. **F** Bubble plots showed ligand-receptor pairs of different $CD8^+$T cell subsets in different treated groups

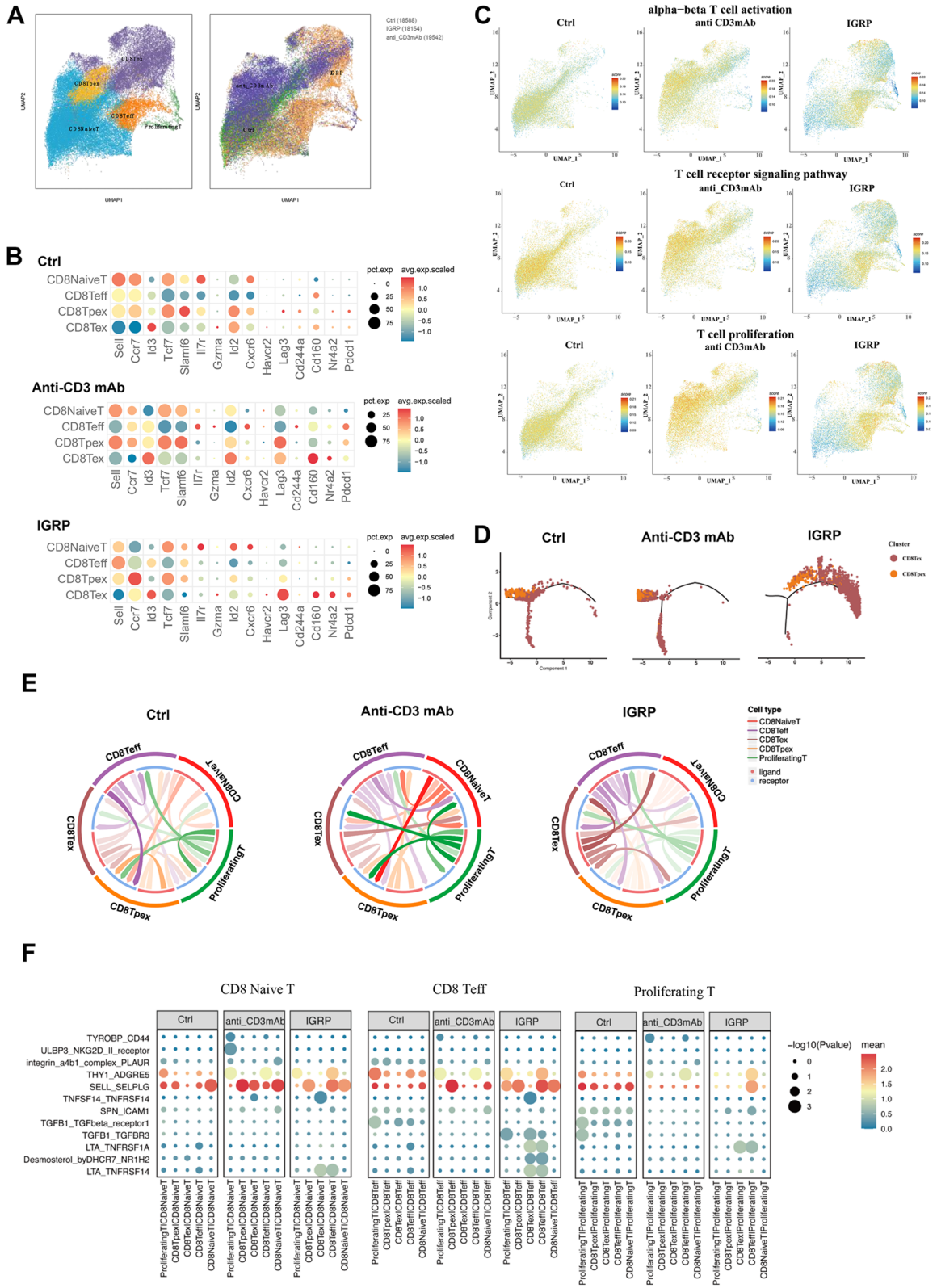

Fig. 8 (See legend on previous page.)

cytokines compared to OA treatment (Fig. 10C–E). These findings suggest that altering mitochondrial fitness may strengthen the exhaustion program in T cells in vitro. Furthermore, compared to anti-CD3 mAb alone, the combined therapy demonstrated higher percentages of total $CD8^+$ exhausted T cells ($P=0.0006$) and TEX cells ($P<0.0001$) (Fig. 10F).

Discussion

Our study explores the diversity of two distinct exhausted $CD8^+$ T-cell subsets in T1D, revealing distinct clinical characteristics, phenotypes, and functions. TCR-sequence and transcriptomic-sequence analyses of these subsets in NOD mice uncovered significant differences in TCR reactivity and metabolic pathways. Both antigen-specific and non-antigen-specific stimuli were found to generate unique exhausted $CD8^+$ T-cell subsets. We identified Lrrk2 as a regulator of mitochondrial fission, influencing the interconversion of exhausted T-cell subsets through phosphorylation of Drp1 at Ser637 and Ser616. Blocking mitochondrial fission with Mdivi-1 was observed to enhance the effectiveness of anti-CD3 mAb immunotherapy by promoting the generation of more terminally exhausted T-cells.

Immunotherapies have become a promising therapeutic strategy for T1D. However, previous researches have shown that not all T1D patients respond uniformly to these treatments. It is plausible that $CD8^+$ T cell exhaustion plays a key role in modulating immune responses against islet β-cells. A recent study suggests that a greater number of exhausted $CD8^+$ T cells may help to slow the progression of β-cell loss [29]. Our research also demonstrated that TEX cells confer protective benefits in T1D but are incapable of differentiating into effector T cells. TPEX cells, which represent an intermediate stage of T cell differentiation, have the potential to develop into either TEX cells or effector T cells. Thus, it is suggested that TPEX cells could be unstable and pathogenic. Supporting this hypothesis, we demonstrated that T1D patients have much fewer total exhausted $CD8^+$ T cells and TEX cells but more TPEX cells. Targeting TPEX cells is therefore important. Furthermore, our findings in both humans and mice indicated that effector $CD8^+$ T cells secrete cytokines at lower levels compared to exhausted $CD8^+$ T cells (data not shown). Similarly, converting mouse TPEX cells into effector T cells yielded equivalent results, which are consistent with the fact that exhausted $CD8^+$ T cells can lead to infections and tumors [22]. This result might be related to their effective exercise of killing target cells ex vivo.

T cell exhaustion results from a variety of signals, including sustained antigen exposure [64]. The principal cytotoxic $CD8^+$ T cells in TME are TEX cells, which have a brief lifespan, while TPEX cells have a longer lifespan and less cytotoxicity [65]. Studies suggest that intense activation of the TCR can lead to terminal exhaustion in tumors for $CD8^+$ T cells, whereas weaker TCR signals may sustain a less mature phenotype [66]. Our research shows that in T1D patients with rapid progression, exposure to a greater variety and potency of antigens increases TEX cells. Conversely, in the natural course of T1D, exposure to self-antigens may lead to more TPEX cells than TEX cells. Identifying the characteristics and mechanisms of distinct exhausted $CD8^+$ T subsets in patients at different stages of T1D could significantly influence the effectiveness of immunotherapy. Our study reveals that TPEX cells are the main subset responsible for the increased proliferation in T1D. Interestingly, we found that their presence is inversely associated with the effectiveness of anti-CD3 mAb therapy. These results imply that TPEX cells have a major impact on T1D therapy outcomes. Therefore, it is crucial to elucidate the mechanisms governing TPEX cell formation and persistence for developing durable immunotherapies for T1D.

Indeed, evidence suggests that the induction of exhausted T cells in T1D is linked to a positive response

(See figure on next page.)

Fig. 9 Blocking mitochondrial fission enhances the efficacy of anti-CD3 mAb immunotherapy in autoimmune diabetic mice. **A** Experimental design for NY8.3 mice immunotherapy studies. Four-week-old female NY8.3 mice ($n=16$/group) were treated with 10 μg anti-CD3mAb or 10 μg anti-CD3mAb in combination with O/A/M every day for 5 days or 20 μg $IGRP_{206–214}$ per nostril daily for 3 days. Mice were sacrificed at day 60 after treatment. **B** The prevalence of diabetes in NY8.3 mice during the course of treatment. **C** At day 60, the percentage of pancreatic islets exhibiting the specified histological scores in "non-diabetic" mice from **A** was measured. Representative pictures of the islets at day 60 "non-diabetic" mice from **A**. Scale bars, 50 μm. **D** TPEX, TEX, and total exhausted $CD8^+$ T cells produced on day 60 were quantified and shown in flow cytograms ($n=8$/group). **E** Experimental design for diabetic NY8.3 mice immunotherapy studies. Diabetic female NY8.3 mice ($n=16$/group) were treated with 10 μg anti-CD3mAb or 10 μg anti-CD3mAb in combination with O/A/M every day for 5 days or 20 μg $IGRP_{206–214}$ per nostril daily for 3 days. Mice were sacrificed at day 30 after treatment. **F** The diabetes remission in diabetic NY8.3 mice after treatment. **G** On day 30, the percentage of pancreatic islets exhibiting the relevant histological score was measured in "non-diabetic" mice from **E**. Representative pictures of the islets at day 30 "non-diabetic" mice from **E**. **H**, **I** total exhausted $CD8^+$ T cells, TPEX, and TEX cells produced on day 30 were quantified and shown in flow cytograms ($n=8$/group). For insulitis, ten pieces per pancreas were blindly scored. (0 = no infiltrate, 1 = 0–25%, 2 = 25–75%, 3 ≥ 75%). White bars, 0; light grey bars, 1; dark grey bars, 2; black bars, 3. *$P<0.05$, **$P<0.01$, ***$P<0.001$, ****$P<0.0001$. One-way ANOVA (**B**, **D**, **F**, **I**). Data represent two independent experiments. Scale bars, 50 μm

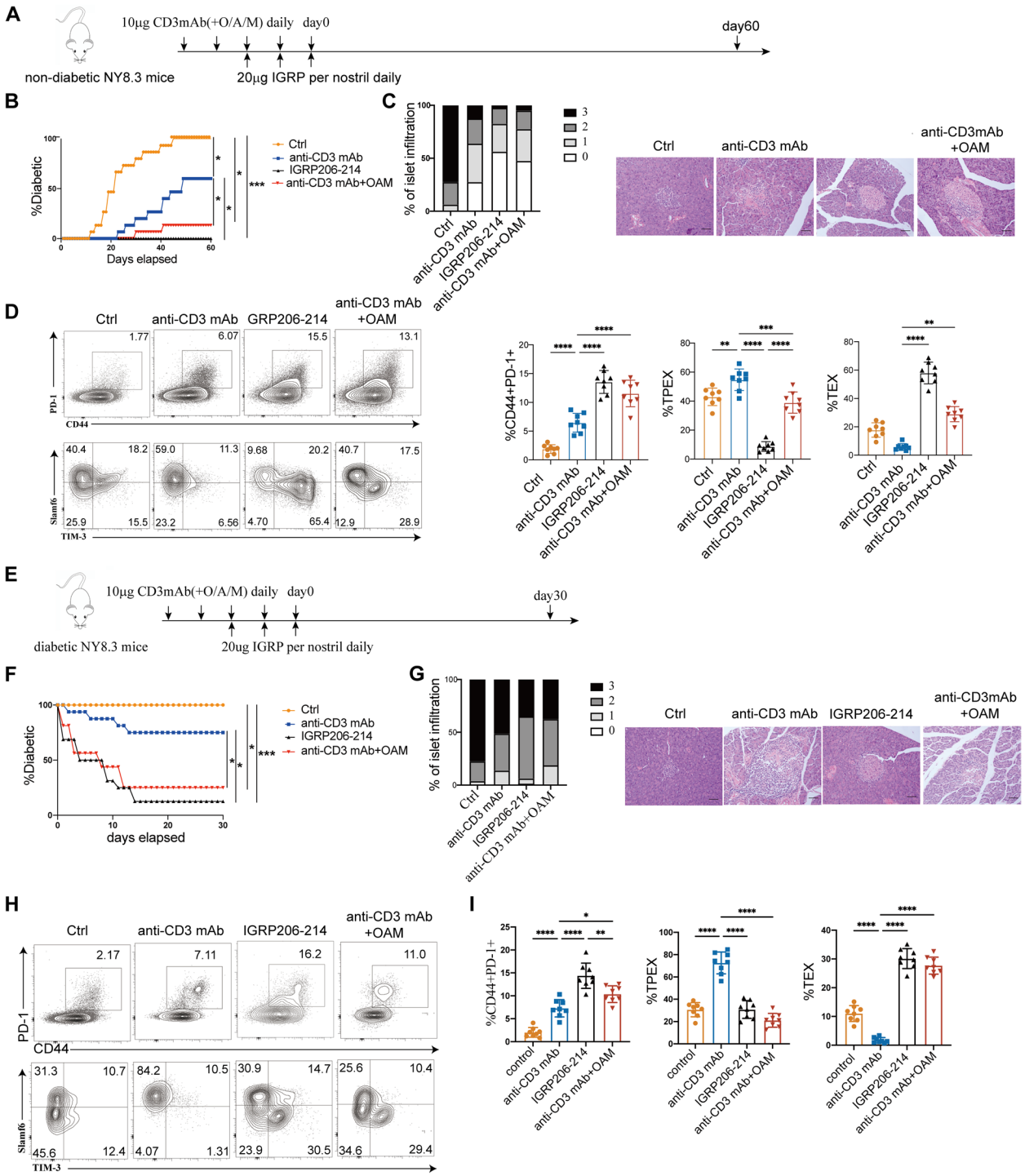

Fig. 9 (See legend on previous page.)

to anti-CD3 mAb treatment [31]. Conversely, the revitalization of exhausted T cells following immune checkpoint receptor blockade has been implicated in the development of T1D in cancer patients [67, 68]. Although monoclonal antibody immunotherapy for T1D can improve islet function, most patients will ultimately experience disease progression. We demonstrated a notable difference between TPEX and TEX cells in their response to immunotherapy. We showed for the first time that antigen-specific immune tolerance primarily induces

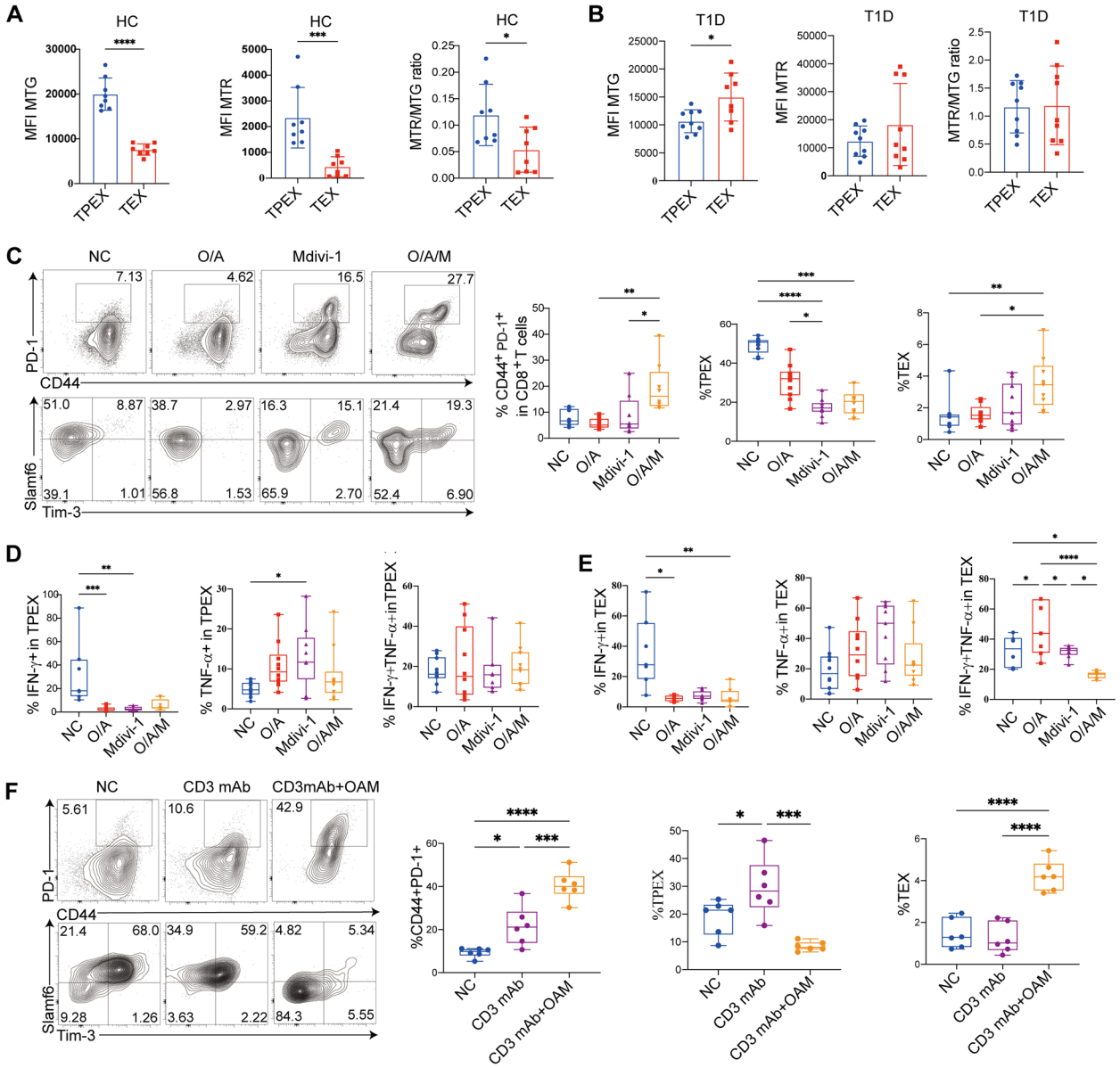

Fig. 10 Combining anti-CD3 mAb and OAM induces TEX cell in T1D patients. MFI variations of ATP5O, CytoC in anti-CD3 unstimulated and stimulated overnight in exhausted and non-exhausted $CD8^+$ T cells or TPEX and TEX cells from PBMCs in T1D patients respectively. MTG, MTR, and normalized ΔΨm (MTR/MTG ratio) in TPEX and TEX cells from PBMCs in controls (**A**) and T1D patients (**B**) respectively. **C** Flow cytograms and analysis of total exhausted $CD8^+$ T cells, TPEX, and TEX cells generated with O/A, Mdivi-1, or O/A/M. Analysis of IFN-γ and TNF-α generated in TPEX cells (**D**) and TEX (**E**) cells with O/A, Mdivi-1, or O/A/M in T1D patients. **F** Flow cytograms and analysis of total exhausted $CD8^+$ T cells, TPEX, and TEX cells generated with anti-CD3mAb, or a combination of anti-CD3mAb and O/A/M in T1D patients. $^*P < 0.05$, $^{**}P < 0.01$, $^{***}P < 0.001$, $^{****}P < 0.0001$. Mann Whitney test (**A,B**); one-way ANOVA (**C–F**). Data represent two independent experiments

more TEX cells. Monoclonal antibody therapy may not induce long-term tolerance due to the induction of more TPEX cells capable of reversing into effector T cells. The significance of mitochondrial dysfunction in human diseases is gaining broader recognition, as it is often associated with increased fragmentation of the mitochondrial network [69]. Mitochondrial homeostasis and energy metabolism are critical for controlling T cell function [25, 70, 71]. We found that subsets of exhausted T cells displayed markedly distinct genes encoding specific mitochondrial proteins. The mitochondrial function of TPEX cells is influenced by Drp1-dependent mitochondrial fission. The primary pro-fission protein, Drp1, has carefully controlled activity to remove damaged mitochondria by

mitophagy. With cycles of fusion and fission, mitochondria are extremely active organelles that can change their shape, distribution, and function [69]. Treatment with oligomycin, antimycin, and Mdivi-1 has shown promising potential for the treatment of various diseases, although these compounds remain at an experimental stage [72–75]. For our experiment, we selected a primary in vivo dosing regimen based on protocols from other disease models. Our study primarily demonstrated the efficacy of these drugs, with no significant adverse effects observed in the mouse tissues. The optimal dosage will be further evaluated in subsequent research. However, the efficacy of the combined anti-CD3 mAb and mdivi-1 treatment has not been validated in patients. Randomized controlled trials (RCTs) are necessary to further validate these findings.

Conclusions

Our findings highlight that subsets of exhausted T cells exhibit distinct phenotypes and functional profiles in T1D. The varying therapeutic outcomes from different immunotherapeutic approaches are likely attributed to the induction of specific exhausted T cell subsets. Our data suggest a novel immunotherapeutic strategy focused on modulating the energy metabolism of exhausted $CD8^+$ T cells, providing new insights to advance clinical immunotherapy in T1D.

Abbreviations

Drp1	Dynamin-related protein 1
FDA	Food and Drug Administration
GAD65	Glutamic acid decarboxylase 65
GSEA	Gene-set enrichment analysis
IA2	Tyrosine phosphatase 2
IACUC	The Institutional Animal Care and Use Committee
Lrrk2	Leucine-rich repeat kinase 2
mAb	Monoclonal antibody
Mdivi-1	Mitochondrial division inhibitor 1
PBMCs	Peripheral blood mononuclear cells
PMA	Phorbol myristic acid
RCTs	Randomized controlled trials
RIPA	Radio immunoprecipitation
scRNA-seq	Single-cell RNA sequencing
T1D	Type 1 diabetes
TCR	T-cell receptor
TEFF	T effector cell
TEX	Terminally exhausted $CD8^+$ T-cells
TPEX	Progenitor exhausted $CD8^+$ T-cells
ZnT8	Zinc transporter 8

Supplementary Information

The online version contains supplementary material available at https://doi.org/10.1186/s12916-025-04001-5.

Additional File 1: Supplementary Materials and Methods.

Additional File 2: Table S1- Characteristics of healthy controls, T1D patients recruited for the study.

Additional File 3: Figures S1-S6. Fig S1- [Correlation between circulating exhausted CD8 + T cells and clinical features]. Fig S2–[Quantification, functionality and Co-receptor expression of exhausted $CD8^+$ T cells in NOD mice]. Fig S3– [Exhausted CD8 + T cells exhibit changes in glucose, lipid, and mitochondrial metabolism in NOD mice]. Fig S4–[Induction of TEX cells by blockade of Mitochondrial fission. $CD44^+PD\text{-}1^+$ exhausted CD8 + T cells]. Fig S5–[Single-cell RNA sequencing was performed on CD8 + T cells from NY8.3 mice 7 days after they were treated with anti-CD3mAb and IGRP206-214]. Fig S6–[Blockade of Mitochondrial fission improves immunotherapy efficacy of anti-CD3 mAb in vitro].

Additional File 4: Original, uncropped gels/blots.

Additional file 5: ARRIVE guidelines.

Additional file 6: the Key Resources Table.

Acknowledgements

We thank Nanjing Medical University Analytical and Testing Center for technical assistance.

Authors' contributions

X.X. conducted the study and wrote the manuscript. X.X. and Y.G. Study design and conceptualization. R.Z.and Z.S.performed the experiments and data analyses. J.G. performed data analyses. H.Z., L.B., Y.C. and Y.J. recruited patients and collected samples. T.Y. supervised the study. All authors reviewed and agreed to the final version of the manuscript.

Funding

This work was supported by grants from the National Natural Science Foundation of China (82270875, 82230028, 82170837, 81770777).

Data availability

No datasets were generated or analysed during the current study.

Declarations

Ethics approval and consent to participate

Ethical approval for the research (including the consent procedure) was granted by the Human Ethics Committee of the First Affiliated Hospital of Nanjing Medical University (No. 2019-SR-121.A1). Experiments were performed in accordance with the regulations of the Institutional Animal Care and Use Committee (IACUC) at Nanjing Medical University.

Consent for publication

Not applicable.

Competing interests

The authors declare no competing interests.

Author details

[1]Department of Endocrinology, The First Affiliated Hospital with Nanjing Medical University, 300 Guangzhou Road, Nanjing, Jiangsu Province, China. [2]Department of Radiation Oncology, The First Affiliated Hospital with Nanjing Medical University, Nanjing, Jiangsu Province, China. [3]Department of Endocrinology, The First People's Hospital of Yancheng, Jiangsu Province, China.

Received: 5 September 2024 Accepted: 12 March 2025
Published online: 31 March 2025

References

1. Pugliese A. Autoreactive T cells in type 1 diabetes. J Clin Invest. 2017;127(8):2881–91.
2. James EA, Pietropaolo M, Mamula MJ. Immune recognition of beta-cells: neoepitopes as key players in the loss of tolerance. Diabetes. 2018;67(6):1035–42.
3. Babon JA, DeNicola ME, Blodgett DM, Crevecoeur I, Buttrick TS, Maehr R, Bottino R, Naji A, Kaddis J, Elyaman W, et al. Analysis of self-antigen specificity of islet-infiltrating T cells from human donors with type 1 diabetes. Nat Med. 2016;22(12):1482–7.

4. Barnett R. Type 1 diabetes. Lancet. 2018;391(10117):195.
5. McKnight JA, Wild SH, Lamb MJ, Cooper MN, Jones TW, Davis EA, Hofer S, Fritsch M, Schober E, Svensson J, et al. Glycaemic control of Type 1 diabetes in clinical practice early in the 21st century: an international comparison. Diabet Med. 2015;32(8):1036–50.
6. Miller KM, Foster NC, Beck RW, Bergenstal RM, DuBose SN, DiMeglio LA, Maahs DM, Tamborlane WV, Network TDEC: Current state of type 1 diabetes treatment in the U.S.: updated data from the T1D Exchange clinic registry. Diabetes Care 2015, 38(6):971–978.
7. Lazar L, Ofan R, Weintrob N, Avron A, Tamir M, Elias D, Phillip M, Josefsberg Z. Heat-shock protein peptide DiaPep277 treatment in children with newly diagnosed type 1 diabetes: a randomised, double-blind phase II study. Diabetes Metab Res Rev. 2007;23(4):286–91.
8. Elias D, Reshef T, Birk OS, van der Zee R, Walker MD, Cohen IR. Vaccination against autoimmune mouse diabetes with a T-cell epitope of the human 65-kDa heat shock protein. Proc Natl Acad Sci U S A. 1991;88(8):3088–91.
9. Demeester S, Keymeulen B, Kaufman L, Van Dalem A, Balti EV, Van de Velde U, Goubert P, Verhaeghen K, Davidson HW, Wenzlau JM, et al. Preexisting insulin autoantibodies predict efficacy of otelixizumab in preserving residual beta-cell function in recent-onset type 1 diabetes. Diabetes Care. 2015;38(4):644–51.
10. Orban T, Bundy B, Becker DJ, DiMeglio LA, Gitelman SE, Goland R, Gottlieb PA, Greenbaum CJ, Marks JB, Monzavi R, et al. Co-stimulation modulation with abatacept in patients with recent-onset type 1 diabetes: a randomised, double-blind, placebo-controlled trial. Lancet. 2011;378(9789):412–9.
11. Pescovitz MD, Greenbaum CJ, Bundy B, Becker DJ, Gitelman SE, Goland R, Gottlieb PA, Marks JB, Moran A, Raskin P, et al. B-lymphocyte depletion with rituximab and beta-cell function: two-year results. Diabetes Care. 2014;37(2):453–9.
12. Rigby MR, Harris KM, Pinckney A, DiMeglio LA, Rendell MS, Felner EI, Dostou JM, Gitelman SE, Griffin KJ, Tsalikian E, et al. Alefacept provides sustained clinical and immunological effects in new-onset type 1 diabetes patients. J Clin Invest. 2015;125(8):3285–96.
13. Herold KC, Bundy BN, Long SA, Bluestone JA, DiMeglio LA, Dufort MJ, Gitelman SE, Gottlieb PA, Krischer JP, Linsley PS, et al. An Anti-CD3 Antibody, Teplizumab, in Relatives at Risk for Type 1 Diabetes. N Engl J Med. 2019;381(7):603–13.
14. Herold KC, Gitelman SE, Ehlers MR, Gottlieb PA, Greenbaum CJ, Hagopian W, Boyle KD, Keyes-Elstein L, Aggarwal S, Phippard D, et al. Teplizumab (anti-CD3 mAb) treatment preserves C-peptide responses in patients with new-onset type 1 diabetes in a randomized controlled trial: metabolic and immunologic features at baseline identify a subgroup of responders. Diabetes. 2013;62(11):3766–74.
15. Hirsch JS. FDA approves teplizumab: a milestone in type 1 diabetes. Lancet Diabetes Endocrinol. 2023;11(1):18.
16. Aronson R, Gottlieb PA, Christiansen JS, Donner TW, Bosi E, Bode BW, Pozzilli P, Group DI. Low-dose otelixizumab anti-CD3 monoclonal antibody DEFEND-1 study: results of the randomized phase III study in recent-onset human type 1 diabetes. Diabetes Care. 2014;37(10):2746–54.
17. Sherry N, Hagopian W, Ludvigsson J, Jain SM, Wahlen J, Ferry RJ Jr, Bode B, Aronoff S, Holland C, Carlin D, et al. Teplizumab for treatment of type 1 diabetes (Protege study): 1-year results from a randomised, placebo-controlled trial. Lancet. 2011;378(9790):487–97.
18. Greenbaum CJ, Schatz DA, Haller MJ, Sanda S. Through the fog: recent clinical trials to preserve beta-cell function in type 1 diabetes. Diabetes. 2012;61(6):1323–30.
19. McLane LM, Abdel-Hakeem MS, Wherry EJ. CD8 T Cell Exhaustion During Chronic Viral Infection and Cancer. Annu Rev Immunol. 2019;37:457–95.
20. Utzschneider DT, Gabriel SS, Chisanga D, Gloury R, Gubser PM, Vasanthakumar A, Shi W, Kallies A. Early precursor T cells establish and propagate T cell exhaustion in chronic infection. Nat Immunol. 2020;21(10):1256–66.
21. Hashimoto M, Kamphorst AO, Im SJ, Kissick HT, Pillai RN, Ramalingam SS, Araki K, Ahmed R. CD8 T Cell Exhaustion in Chronic Infection and Cancer: Opportunities for Interventions. Annu Rev Med. 2018;69:301–18.
22. Wherry EJ, Kurachi M. Molecular and cellular insights into T cell exhaustion. Nat Rev Immunol. 2015;15(8):486–99.
23. Sen DR, Kaminski J, Barnitz RA, Kurachi M, Gerdemann U, Yates KB, Tsao HW, Godec J, LaFleur MW, Brown FD, et al. The epigenetic landscape of T cell exhaustion. Science. 2016;354(6316):1165–9.
24. Scott-Browne JP, Lopez-Moyado IF, Trifari S, Wong V, Chavez L, Rao A, Pereira RM. Dynamic Changes in Chromatin Accessibility Occur in CD8(+) T Cells Responding to Viral Infection. Immunity. 2016;45(6):1327–40.
25. Bengsch B, Johnson AL, Kurachi M, Odorizzi PM, Pauken KE, Attanasio J, Stelekati E, McLane LM, Paley MA, Delgoffe GM, et al. Bioenergetic Insufficiencies Due to Metabolic Alterations Regulated by the Inhibitory Receptor PD-1 Are an Early Driver of CD8(+) T Cell Exhaustion. Immunity. 2016;45(2):358–73.
26. Beltra JC, Manne S, Abdel-Hakeem MS, Kurachi M, Giles JR, Chen Z, Casella V, Ngiow SF, Khan O, Huang YJ, et al. Developmental relationships of four exhausted CD8(+) T cell subsets reveals underlying transcriptional and epigenetic landscape control mechanisms. Immunity. 2020;52(5):825-841 e828.
27. Miller BC, Sen DR, Al Abosy R, Bi K, Virkud YV, LaFleur MW, Yates KB, Lako A, Felt K, Naik GS, et al. Subsets of exhausted CD8(+) T cells differentially mediate tumor control and respond to checkpoint blockade. Nat Immunol. 2019;20(3):326–36.
28. McKinney EF, Lee JC, Jayne DR, Lyons PA, Smith KG. T-cell exhaustion, co-stimulation and clinical outcome in autoimmunity and infection. Nature. 2015;523(7562):612–6.
29. Wiedeman AE, Muir VS, Rosasco MG, DeBerg HA, Presnell S, Haas B, Dufort MJ, Speake C, Greenbaum CJ, Serti E, et al. Autoreactive CD8+ T cell exhaustion distinguishes subjects with slow type 1 diabetes progression. J Clin Invest. 2020;130(1):480–90.
30. Abdelsamed HA, Zebley CC, Nguyen H, Rutishauser RL, Fan Y, Ghoneim HE, Crawford JC, Alfei F, Alli S, Ribeiro SP, et al. Beta cell-specific CD8(+) T cells maintain stem cell memory-associated epigenetic programs during type 1 diabetes. Nat Immunol. 2020;21(5):578–87.
31. Long SA, Thorpe J, DeBerg HA, Gersuk V, Eddy J, Harris KM, Ehlers M, Herold KC, Nepom GT, Linsley PS. Partial exhaustion of CD8 T cells and clinical response to teplizumab in new-onset type 1 diabetes. Sci Immunol. 2016;1(5):eaai7793.
32. Perdigoto AL, Preston-Hurlburt P, Clark P, Long SA, Linsley PS, Harris KM, Gitelman SE, Greenbaum CJ, Gottlieb PA, Hagopian W, et al. Treatment of type 1 diabetes with teplizumab: clinical and immunological follow-up after 7 years from diagnosis. Diabetologia. 2019;62(4):655–64.
33. Diggins KE, Serti E, Muir V, Rosasco M, Lu T, Balmas E, Nepom G, Long SA, Linsley PS. Exhausted-like CD8+ T cell phenotypes linked to C-peptide preservation in alefacept-treated T1D subjects. JCI Insight. 2021;6(3):e142680.
34. Pearce EL, Pearce EJ. Metabolic pathways in immune cell activation and quiescence. Immunity. 2013;38(4):633–43.
35. Chang CH, Pearce EL. Emerging concepts of T cell metabolism as a target of immunotherapy. Nat Immunol. 2016;17(4):364–8.
36. American Diabetes Association Professional Practice C: 2. Classification and diagnosis of diabetes: standards of medical care in diabetes-2022. Diabetes Care 2022, 45(Suppl 1):S17–S38.
37. Pertea M, Kim D, Pertea GM, Leek JT, Salzberg SL. Transcript-level expression analysis of RNA-seq experiments with HISAT StringTie and Ballgown. Nat Protoc. 2016;11(9):1650–67.
38. Robinson MD, McCarthy DJ, Smyth GK. edgeR: a Bioconductor package for differential expression analysis of digital gene expression data. Bioinformatics. 2010;26(1):139–40.
39. Wolf FA, Angerer P, Theis FJ. SCANPY: large-scale single-cell gene expression data analysis. Genome Biol. 2018;19(1):15.
40. Butler A, Hoffman P, Smibert P, Papalexi E, Satija R. Integrating single-cell transcriptomic data across different conditions, technologies, and species. Nat Biotechnol. 2018;36(5):411–20.
41. Efremova M, Vento-Tormo M, Teichmann SA, Vento-Tormo R. Cell PhoneDB: inferring cell-cell communication from combined expression of multi-subunit ligand-receptor complexes. Nat Protoc. 2020;15(4):1484–506.
42. Andreatta M, Carmona SJ. UCell: Robust and scalable single-cell gene signature scoring. Comput Struct Biotechnol J. 2021;19:3796–8.
43. Qiu X, Hill A, Packer J, Lin D, Ma YA, Trapnell C. Single-cell mRNA quantification and differential analysis with Census. Nat Methods. 2017;14(3):309–15.
44. Robson NC, Beacock-Sharp H, Donachie AM, Mowat AM. Dendritic cell maturation enhances CD8+ T-cell responses to exogenous antigen via a proteasome-independent mechanism of major histocompatibility complex class I loading. Immunology. 2003;109(3):374–83.

45. Jensen SS, Gad M. Differential induction of inflammatory cytokines by dendritic cells treated with novel TLR-agonist and cytokine based cocktails: targeting dendritic cells in autoimmunity. J Inflamm (Lond). 2010;7: 37.
46. Thommen DS, Koelzer VH, Herzig P, Roller A, Trefny M, Dimeloe S, Kiialainen A, Hanhart J, Schill C, Hess C, et al. A transcriptionally and functionally distinct PD-1(+) CD8(+) T cell pool with predictive potential in non-small-cell lung cancer treated with PD-1 blockade. Nat Med. 2018;24(7):994–1004.
47. Niu X, Li S, Li P, Pan W, Wang Q, Feng Y, Mo X, Yan Q, Ye X, Luo J, et al. Longitudinal Analysis of T and B Cell Receptor Repertoire Transcripts Reveal Dynamic Immune Response in COVID-19 Patients. Front Immunol. 2020;11: 582010.
48. Dura B, Choi JY, Zhang K, Damsky W, Thakral D, Bosenberg M, Craft J, Fan R. scFTD-seq: freeze-thaw lysis based, portable approach toward highly distributed single-cell 3' mRNA profiling. Nucleic Acids Res. 2019;47(3): e16.
49. Sherry NA, Chen W, Kushner JA, Glandt M, Tang Q, Tsai S, Santamaria P, Bluestone JA, Brillantes AM, Herold KC. Exendin-4 improves reversal of diabetes in NOD mice treated with anti-CD3 monoclonal antibody by enhancing recovery of beta-cells. Endocrinology. 2007;148(11):5136–44.
50. Daniel D, Wegmann DR. Protection of nonobese diabetic mice from diabetes by intranasal or subcutaneous administration of insulin peptide B-(9–23). Proc Natl Acad Sci U S A. 1996;93(2):956–60.
51. Franchi L, Monteleone I, Hao LY, Spahr MA, Zhao W, Liu X, Demock K, Kulkarni A, Lesch CA, Sanchez B, et al. Inhibiting Oxidative Phosphorylation In Vivo Restrains Th17 Effector Responses and Ameliorates Murine Colitis. J Immunol. 2017;198(7):2735–46.
52. Yeh CT, Su CL, Huang CY, Lin JK, Lee WH, Chang PM, Kuo YL, Liu YW, Wang LS, Wu CH, et al. A preclinical evaluation of antimycin a as a potential antilung cancer stem cell agent. Evid Based Complement Alternat Med. 2013;2013: 910451.
53. Liu JM, Yi Z, Liu SZ, Chang JH, Dang XB, Li QY, Zhang YL. The mitochondrial division inhibitor mdivi-1 attenuates spinal cord ischemia-reperfusion injury both in vitro and in vivo: Involvement of BK channels. Brain Res. 2015;1619:155–65.
54. Wolfl M, Kuball J, Ho WY, Nguyen H, Manley TJ, Bleakley M, Greenberg PD. Activation-induced expression of CD137 permits detection, isolation, and expansion of the full repertoire of CD8+ T cells responding to antigen without requiring knowledge of epitope specificities. Blood. 2007;110(1):201–10.
55. Chen Z, Ji Z, Ngiow SF, Manne S, Cai Z, Huang AC, Johnson J, Staupe RP, Bengsch B, Xu C, et al. TCF-1-centered transcriptional network drives an effector versus exhausted CD8 T cell-fate decision. Immunity. 2019;51(5):840-855 e845.
56. Yu YR, Imrichova H, Wang H, Chao T, Xiao Z, Gao M, Rincon-Restrepo M, Franco F, Genolet R, Cheng WC, et al. Disturbed mitochondrial dynamics in CD8(+) TILs reinforce T cell exhaustion. Nat Immunol. 2020;21(12):1540–51.
57. Franco F, Jaccard A, Romero P, Yu YR, Ho PC. Metabolic and epigenetic regulation of T-cell exhaustion. Nat Metab. 2020;2(10):1001–12.
58. Baechler BL, Bloemberg D, Quadrilatero J. Mitophagy regulates mitochondrial network signaling, oxidative stress, and apoptosis during myoblast differentiation. Autophagy. 2019;15(9):1606–19.
59. Mao H, Chen W, Chen L, Li L. Potential role of mitochondria-associated endoplasmic reticulum membrane proteins in diseases. Biochem Pharmacol. 2022;199: 115011.
60. Pfanner N, Warscheid B, Wiedemann N. Mitochondrial proteins: from biogenesis to functional networks. Nat Rev Mol Cell Biol. 2019;20(5):267–84.
61. Kraus F, Roy K, Pucadyil TJ, Ryan MT. Function and regulation of the divisome for mitochondrial fission. Nature. 2021;590(7844):57–66.
62. Archer SL. Mitochondrial dynamics–mitochondrial fission and fusion in human diseases. N Engl J Med. 2013;369(23):2236–51.
63. Ko HJ, Tsai CY, Chiou SJ, Lai YL, Wang CH, Cheng JT, Chuang TH, Huang CF, Kwan AL, Loh JK, et al. The phosphorylation status of Drp1-Ser637 by PKA in mitochondrial fission modulates mitophagy via PINK1/Parkin to exert multipolar spindles assembly during mitosis. Biomolecules. 2021;11(3):424–48.
64. Utzschneider DT, Alfei F, Roelli P, Barras D, Chennupati V, Darbre S, Delorenzi M, Pinschewer DD, Zehn D. High antigen levels induce an exhausted phenotype in a chronic infection without impairing T cell expansion and survival. J Exp Med. 2016;213(9):1819–34.
65. Horton BL, Williams JB, Cabanov A, Spranger S, Gajewski TF. Intratumoral CD8(+) T-cell apoptosis is a major component of t-cell dysfunction and impedes antitumor immunity. Cancer Immunol Res. 2018;6(1):14–24.
66. Burger ML, Cruz AM, Crossland GE, Gaglia G, Ritch CC, Blatt SE, Bhutkar A, Canner D, Kienka T, Tavana SZ, et al. Antigen dominance hierarchies shape TCF1(+) progenitor CD8 T cell phenotypes in tumors. Cell. 2021;184(19):4996-5014 e4926.
67. Stamatouli AM, Quandt Z, Perdigoto AL, Clark PL, Kluger H, Weiss SA, Gettinger S, Sznol M, Young A, Rushakoff R, et al. Collateral damage: insulin-dependent diabetes induced with checkpoint inhibitors. Diabetes. 2018;67(8):1471–80.
68. Hughes J, Vudattu N, Sznol M, Gettinger S, Kluger H, Lupsa B, Herold KC. Precipitation of autoimmune diabetes with anti-PD-1 immunotherapy. Diabetes Care. 2015;38(4):e55-57.
69. Pernas L, Scorrano L. Mito-morphosis: mitochondrial fusion, fission, and cristae remodeling as key mediators of cellular function. Annu Rev Physiol. 2016;78:505–31.
70. Fisicaro P, Barili V, Montanini B, Acerbi G, Ferracin M, Guerrieri F, Salerno D, Boni C, Massari M, Cavallo MC, et al. Targeting mitochondrial dysfunction can restore antiviral activity of exhausted HBV-specific CD8 T cells in chronic hepatitis B. Nat Med. 2017;23(3):327–36.
71. Mills EL, Kelly B, O'Neill LAJ. Mitochondria are the powerhouses of immunity. Nat Immunol. 2017;18(5):488–98.
72. Georgakopoulos ND, Wells G, Campanella M. The pharmacological regulation of cellular mitophagy. Nat Chem Biol. 2017;13(2):136–46.
73. Ogita M, Ogita A, Usuki Y, Fujita K, Tanaka T. Antimycin A-induced cell death depends on AIF translocation through NO production and PARP activation and is not involved in ROS generation, cytochrome c release and caspase-3 activation in HL-60 cells. J Antibiot (Tokyo). 2009;62(3):145–52.
74. Scherbakov AM, Sorokin DV, Omelchuk OA, Shchekotikhin AE, Krasil'nikov MA. Glucose starvation greatly enhances antiproliferative and antiestrogenic potency of oligomycin A in MCF-7 breast cancer cells. Biochimie. 2021;186:51–8.
75. Liang X, Wang S, Wang L, Ceylan AF, Ren J, Zhang Y. Mitophagy inhibitor liensinine suppresses doxorubicin-induced cardiotoxicity through inhibition of Drp1-mediated maladaptive mitochondrial fission. Pharmacol Res. 2020;157: 104846.

Publisher's Note